PREDICTION OF THE HIP JOINT CENTRE BY PREDICTIVE METHODS, FUNCTIONAL METHODS AND ULTRASOUND IMAGING TECHNIQUE

By Taranjit Kaur Romana

This thesis is submitted in partial fulfilment of the requirements for the degree of

MSc in Bioengineering

21st August 2012

Bioengineering Unit

University of Strathclyde

Glasgow, UK

This thesis is the result of the author's original research. It has been composed by the author and has not been previously submitted for examination which has led to the award of degree.

Signed:

Date:

ACKNOWLEDGEMENTS

I am thankful to my project supervisor Mr. Stephanos Solomonidis for all the help, guidance and support he provided throughout the duration of the project, showing great patience along the way. He was always available when I needed his help or advice. He always went out of the way and helped me to implement new ideas for the project.

I also would like to thank my Co-supervisor Prof. Oleg Davydov who helped me understand MATLAB and provided much needed help and support in the development of the code. He has shown a great interest by coming up with different methods to improve the results throughout the duration of the project.

A huge thank you to Prof. George Corner who came all the way from Dundee and helped me understand Ultrasound in a much better way which proved very useful to obtain better results. He also allowed us to use the ultrasound facilities at the Ninewells hospital where he works. That was a kind gesture from his side which was greatly appreciated.

I would also like to thank the two subjects who were very sporty and helpful in all the ways. Without them this project would not have been such a success. Lastly, I would like to thank all the departmental staff for constantly supported me and my classmates and my family for keeping my spirits high throughout the course, couldn't have done without you.

ABSTRACT

To study joint kinetics and kinematics during gait analysis, it is necessary that the position of the Hip Joint Centre (HJC) from a point in a local frame of reference is determined as accurately as possible. Various studies have stated that failure to do so results in errors up to 20% in joint kinematics. It is difficult to obtain the exact location of the HJC as it is very deeply seated inside the body with a lot of tissue and muscle layers coverings. The theories that attempt to locate the HJC accurately are either predictive or functional methods.

The predictive methods that are extensively used in clinical settings use set of regression equations based on pelvic geometry and leg length. The functional methods include the sphere fit techniques which reduce the errors as compared to the regression equations but both the methods are greatly affected by Soft Tissue Artefacts.

This study performs a comparison between the predictive and functional methods by exploring the ultrasound imaging a validation technique. The findings suggested that all the current validation techniques are subject to errors due to soft tissue artefacts which led to erroneous location of the HJC. The predictive methods proved to be the least accurate which was disturbing because they are widely used in clinics as a method to locate the HJC.

TABLE OF CONTENTS

CHAPTER 1.

INTRODUCTION

1.1. BACKGROUND

Gait analysis study refers to the study of walking patterns of people, evaluating the spatial-temporal components and joint kinematics. Calculation of joint reaction forces needs the accurate location of joint angles which can be easily determined for some joints like knee and ankle but it becomes challenging to locate the more deeply seated joints like the hip joint. The hip joint is surrounded by a considerable amount of soft tissue and the methods to locate the exact position of the hip joint suffer from artefacts due to this soft tissue which makes it difficult to locate the hip joint. The soft tissue artefacts refer to the soft tissue movement in relation to the underlying bone. They have been known to affect all the methods that aim to evaluate the exact location of the Hip joint centre.

Gait analysis studies have been around for a while now. Amongst all the methods evolved over the years, two methods - predictive and functional methods have shown remarkable results. The predictive method is one of the first methods which rely on the regression equations for determining the location of Hip Joint Centre that are based on pelvic geometry and leg length. But it was proved later that these equations do not provide accurate results, the reason being variations in anatomical geometry of individuals (Leardini, et al., 1999). Despite the inaccuracies in calculating the hip joint centre, these regression equations are still used in clinical settings. The regression equations used in the present study are given by Harrington, et al., (2007) which are supposed to be the most accurate till date and are widely used in clinics.

Various functional methods were developed recently to reduce and overcome the errors found in predictive methods. Leardini et al. (1999) summarised the idea of functional method described by Aurelio Cappozzo in 1984, suggesting the hip joint as a pivot point for the movement of femur in relation to pelvis. All functional methods assume hip joint as a ball - socket joint with the centre of the femoral head as the joint centre, which allows the femur to move with respect to the pelvis, to be modelled as a sphere. Markers are attached on the bony landmarks on the skin and their trajectories are tracked over time. Study by Gamage & Lasenby, (2002) incorporates a similar method which has been used to create an algorithm for the present study. The execution of the above mentioned technique is discussed in later sections.

Owing to their customizable nature, the issue of individual subject's geometry was overcome by the functional methods which proved a great advantage over the predictive methods. The functional methods have not been as popular as the predictive methods in clinical settings due to the high expenses involved in setting up the equipment for them (Harrington, et al., 2007). Functional methods showed significant improvements but were greatly affected by soft tissue artefacts because the motion of the markers that were placed on the skin surface was found to be unsynchronized with the underlying bone. This led to incorrect modelling of the spheres that represented motion of femur relative to the pelvis which in turn provided inaccurate joint location.

1.2 AIM

A study conducted in 2011 by Craig Simpson predicted the Hip Joint Centre by using predictive and functional methods along with validation techniques like ultrasound and MRI to determine the HJC. It was a follow up study to the one that was conducted in 2010 by Paul Byrne. The predictive and functional methods adopted were the regression equations described by Harrington, et al., (2007) and Gamage &

Lasenby, (2002) respectively. Tests incorporating the functional method were performed on a mechanical model which eliminated soft tissue artefacts and then the same tests were performed with subjects analysing the effects of STA on the prediction of HJC. The developments of functional methods gave improved results but were still not sufficiently accurate. Unfortunately, the predictive method contrary to its reputation turned out to be the least accurate. The validation procedure using ultrasound gave fairly useful results but they vastly differed from those given by MRI. Results from MRI were considered to be the most accurate, as the images were clearer. However, both these techniques were largely affected by Soft Tissue Artefacts (Simpson, 2011).

The effects of Soft Tissue Artefacts on HJC are still unknown. Also it is seen that the STA is different for each individual. This causes appreciable error that cannot be ignored. This study will be in continuation to Simpson's (2011) study. It aims at determining and minimising the STA by analysing the mechanical model data and improvising it to implement it on human subject in order locate the HJC more accurately. The results will be compared to the regression equations given by Harrington, et al., (2007) in order to assess its accuracy. The result that was obtained from MRI by Simpson, (2011) will be used as true co-ordinates of the HJC for the present project. However, the technique of MRI is costly and time consuming and thus cannot be used as frequently as ultrasound which is more practicable. Thus, the present project would further explore various ultrasound imaging techniques along with analysing the mechanical model in more detail.

CHAPTER 2.

LITERATURE REVIEW

2.1 ANATOMY OF THE HIP JOINT AND SIGNIFICANCE OF ACCURATE LOCATION OF HIP JOINT CENTRE

Due to its deep location within the body which makes it difficult to palpate the hip joint, the location of its centre has not been determined accurately till now. The hip joint has symmetrical concave and convex parts of the acetabulum and head of femur making a perfect ball and socket joint. Between the two surfaces, a padding of fibrous cartilage forms a lubrication which is much needed during the joint movements (Martini & Nath, 2009). The axis system relating the pelvis to the femur which is also used for the present study was produced by Wu, et al., (2002). In the system, Wu, et al., (2002) used HJC as the origin for both femoral and pelvic systems. In addition to this, a 2nd axis (proximal/distal) was determined relating the HJC to the midpoint of the two epicondyles of the femur. Both the systems are depicted in the figure below.

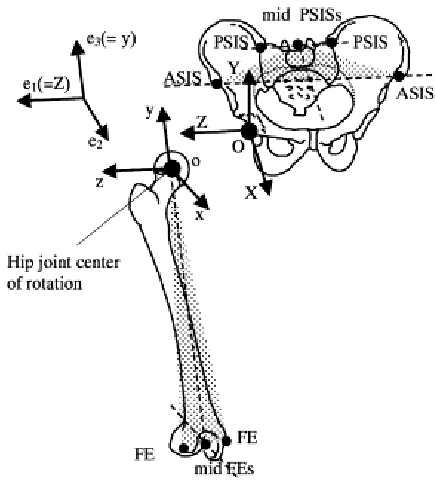

Figure 2.1 – Pelvic and Femoral Axis System (Wu, 2002)

For computation of hip kinetics and kinematics and for determination of the moment forces crossing the hip, accurate location of the hip joint centre is essential. Clinically the results of predictive and functional methods are being used and many studies involving these methods have been conducted in order to predict the accurate location of the hip joint centre but none have succeeded in doing so without significant amount of errors. These errors are mainly due to soft tissue artefact (STA). The latest predictive method involving the regression equations given by Harrington, et al., (2007) used MRI to locate the hip joint centre in children, adults and patients with cerebral palsy. The regression equations incorporated the pelvic width and pelvic depth which were generalised over the three subject groups. The equations were known to improve the accuracy of locating HJC up to 7 mm as compared to the earlier regression equations. But, the authors do not take into account the pelvic asymmetries, errors in marker placement and soft tissue artefacts (Harrington, et al., 2007). These parameters are found to affect the results significantly and should not be ignored.

2.2 TECHNIQUES COMPARING THE ACCURACY OF PREDICTIVE AND FUNCTIONAL METHODS

Recently in 2011, Sangeux, et al., attempted to compare the accuracy of the hip joint centre localisation from two predictive methods and five functional methods against 3-D ultrasound (3-DUS) on 19 normal subjects. The 3-DUS determined the location of the hip joint centre anatomically. The two predictive methods that were used were a software incorporating PIG (Plug In Gait) - the most widely applicable method in clinical gait analysis, derived from the study of Davis, et al., (1991) and the other included the regression equations reported by Harrington, et al., (2007) which is the most recent one. Both these methods use different anthropometric measurements. The first method used the inter-ASIS distance, leg length, and the distance between the greater trochanter and the ipsilateral ASIS. While the other method used measurements of pelvic depth, width and height.

The five functional methods that were used in this study consisted of 2 sphere fitting (geometric and algebric) and 2 transformation methods (Centre Transformation Technique – CTT and Symmetrical Centre of rotation Estimation - SCORE) and a global calibration method. The authors do not clearly elaborate on the two transformation techniques that are used. Matlab 'minFunc' function was used to iteratively solve geometric sphere fit and SCORE algorithms. Solving algebraic and CTT algorithms was done by using their closed form equations. The global method used the software by VICON which uses a 5 segment (pelvis, thighs and shanks), 4 joint, rigid body model with 3 doF hips (adduction, flexion and internal rotation) and 2 doF knees (flexion and internal rotation). The figure below shows the marker set used for this study.

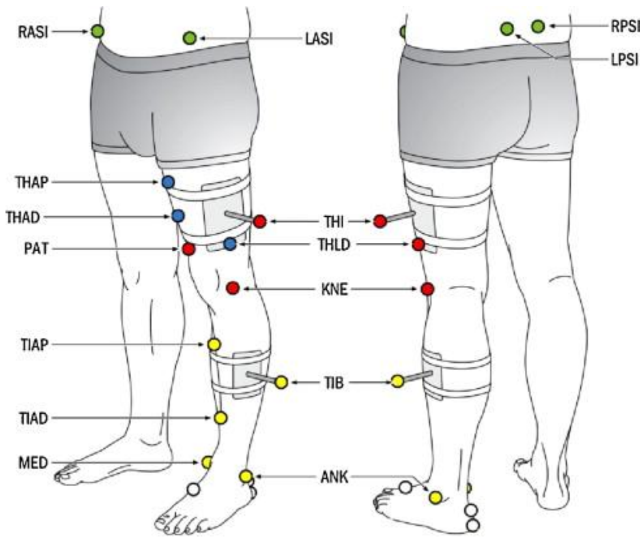

Fig.2.2 - Marker set definition. (Sanguex, et al., 2011)

A previous study by Peters, et al., (2010) described and validated the 3-DUS method for anatomically locating the HJC that is used in this study. The probe had markers attached to it that enabled the probe's image plane position to be within the same pelvic coordinate system. The probe was kept on the upper thigh in an anterio-medial direction to image the femoral head. A least squares method determined the femoral head centre within the pelvic coordinate system. This method was compared with MRI data in an earlier study that suggested an accuracy of 4 ± 2 mm.

The results of this study revealed that the sphere fitting techniques outperformed the functional methods with the geometric techniques giving slightly better results than algebraic. They provided the best results with an average error of 15mm and 85% of hips being within 20mm of the 3-DUS measurement. These results are not very convincing because a 15 mm error seems to be a big number. It is not very clear as to how with such a big error the authors claim to have 85% of the hips within 20 mm. This study claims to be the first one to have compared the transformation techniques for HJC localization to the reference position in images obtained from medical imaging techniques. The following table compares some previous studies with the current one. As expected, the PIG performed badly whereas the equations from Harrington, et al., (2007) gave almost exact results as the best functional calibration technique showing a mean absolute error of 16mm and 88% of measurements being within 20mm. Also the study confirmed that modelling STA as Gaussian noise does not represent the limitations of the functional calibration techniques adequately and conclusions based upon its use cannot be accurate. Thus, it is very evident that inaccuracy in the location of hip joint centre can have remarkable effects on gait analysis studies.

Reference		*N* subject	BMI (kg/m^2)	Functional (mm)	Davis et al. (mm)	Harrington et al. (mm)
Bell et al.	X-Ray	7	26.2	38 ± 19		
Leardini et al.	X-Ray	11	23.7 ± 2.8	12 ± 4	29 ± 8	
Hicks and Richards	3-DUS	9	NS	13 ± 4		
(Sangeux, et al., 2011)	3-DUS	19	23.0 ± 3.6	15 ± 5	30 ± 6	16 ± 6

Table 1. Comparison of the average distance (mm) of the HJC localization against a medical image based reference. (Sanguex, et al., 2011)

In another study by Seidel, et al., (1995) 65 human cadaveric pelves were examined (35 female and 30 male) and an anatomical anthropometric study was performed in order to study the relationship between HJC and few chosen aspects of pelvic geometry. The objective of this study was to know whether the error in estimating Hip Joint Centre along each axis is minimized with fixed percentages of single pelvic parameter as found out by Bell, et al., (1989, 1990) or whether other pelvic measurements are required to locate the HJC more precisely. The study also aimed at answering the question of whether the gender and the corresponding differences in pelvic shape effect HJC estimation.

Bell, et al., (1989, 1990) and Seidel, et al., (1995) suggest the same method for locating the hip joint centre in the mediolateral axis as 14% of PW (mean error 0.58

cm) relative to ASIS. But, Seidel, et al., (1995) reveals through correlation analysis that the location of the HJC cannot be expressed correctly as a function of PW alone and that it needs estimation as a function of PH -pelvic height and PD - pelvic depth also. The pelvic width was measured from right to left ASIS; pelvic height was the upright distance from pubic centre to the inter-ASIS line at 90 degrees and pelvic depth was measured by a calliper accurate to a millimetre from the ASIS to the PSIS in an oblique manner.

With ASIS position known, HJC-x is the projection of the hip joint centre onto the frontal plane, HJC-y is the medial measurement and HJC-z is the measure of height. The figures for correlation of HJC-x and HJC-z are shown below.

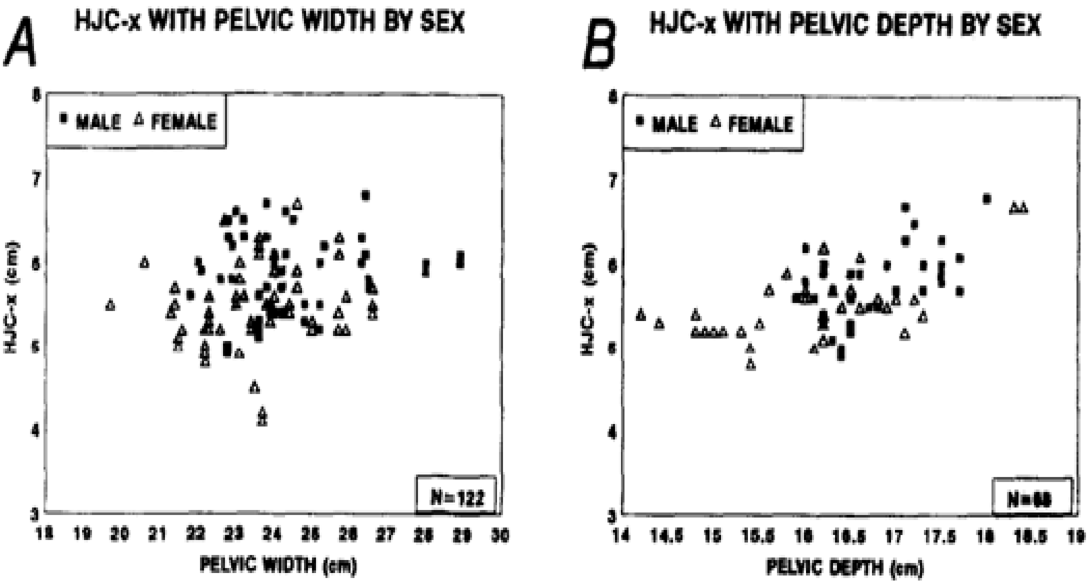

Figure 2.3 - Plots of HJC-x with pelvic width and pelvic depth by gender in centimetres. (Seidel, et al., 1995)

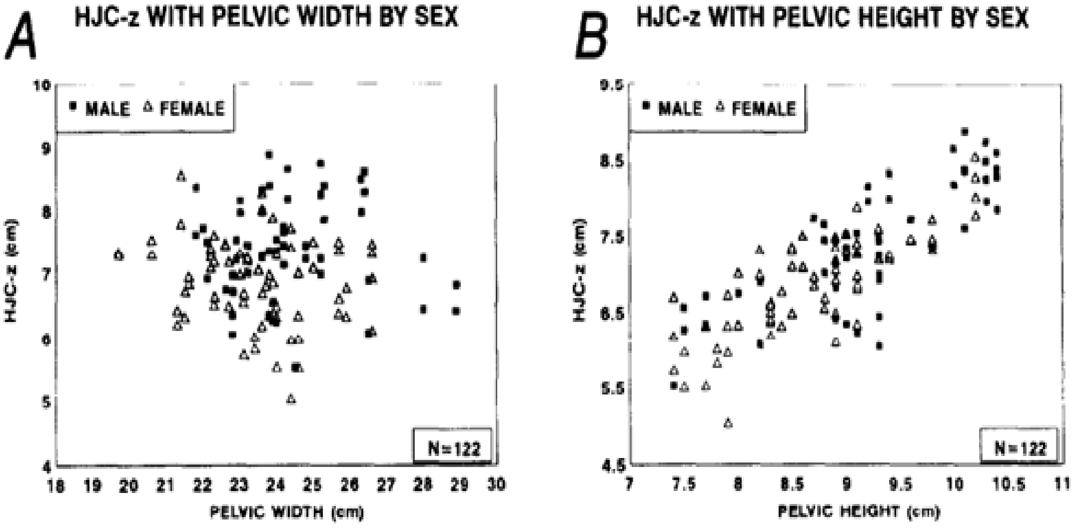

Figure 2.4 - Plots of HJC-z with pelvic width and pelvic height by gender in centimetres. (Seidel, et al., 1995)

Findings suggested that pelvic width correlated well with pelvic depth and it is seen that HJC-x does not correlate with pelvic width but correlates greatly with pelvic depth. Similarly, from the second figure, HJC-z is highly correlated with pelvic height. There was no significant relationship found between the pelvic width and pelvic height or pelvic height and pelvic depth. Also, HJC-x and HJC-y do not correlate well with pelvic height and HJC-y and HJC-z do not significantly correlate with pelvic depth. But from the figures, it can be seen that HJC-x correlates better with PD than with PW but it is not a very high correlation, similar for HJC-z.

Study by Bell, et al., (1989, 1990) found out the HJC location to be 30% distal, 14% medial and 22% posterior to the ASIS. These results were evaluated with respect to pelvic width alone as the function. But Seidel, et al., (1995) found out the HJC location with all three pelvic parameters as a function. With respect to ASIS the HJC was found to be 14% (mean error 0.58 cm/ S.D. 3%) of pelvic width medially, 34% (mean error 0.30 cm/ S.D. 2%) of pelvic depth posteriorly and 79% (mean error 0.35

cm/ S.D. 5%) of pelvic height inferiorly. No important differences were seen between male and female pelves in HJC estimation.

2.3 SOFT TISSUE ARTEFACTS AND ITS ASSESSMENT

Optoelectronic stereophotogrammetry is another technique that has been used to analyse human motion. Soft tissue artefacts affect this technique due to an incorrect assumption that the markers on the skin are firmly attached to the underlying bones (Stagni, et al., 2005). Stagni, et al., (2005) studied two subjects with total knee replacement who were supposed to undergo data acquisition along with with fluoroscopy and stereophotogrammetry during different activities of daily living that included knee extension, sit/stand and vice versa, step up-down and stair climbing. Fluoroscopy is a technique for viewing real time moving images of the internal structures of a body by using X-ray source and fluorescent screen on either side of the subject (U.S. Department of Health and Human Services, 2012). The study aimed at quantifying STA on the thigh and shank by a novel technique combining traditional stereophotogrammetry and reconstruction of 3D kinematics from fluoroscopic images. Tracking of the prosthesis components by fluoroscopy was used to reconstruct the reference 3D kinematics of the femur and tibia. STA was quantified fully in 3D for the first time without any restriction to skin movement during daily living activities in the thigh and shank. STA was quantified with the help of optoelectronic stereophotogrammetry by tracking the movement of a grid of retro-reflecting markers on the thigh and shank in relation to the bones. Evaluation of the propagation of STA to the knee rotations was also done. The findings showed that the displacement or standard deviation of the skin markers in the respective anatomical frames were greater on thigh (31mm) than on shank (21mm) along the medio-lateral direction. STA propagation mostly affected the ab/adduction (RMS errors up to192%) and int/external (RMS errors up to 117%) knee rotation angles. The study concluded that flexion/extension calculations at knee through external markers can be considered reliable but not internal/external and abduction/adduction and also that STA are both task and subject dependent.

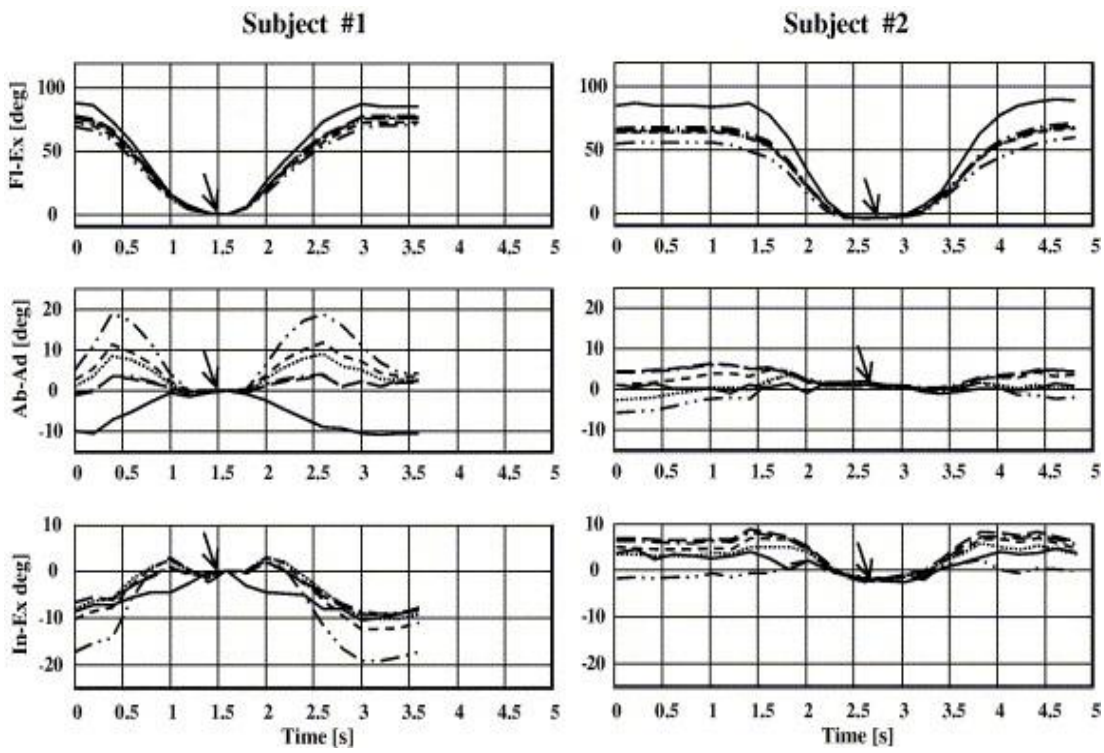

Figure 2.6 - Knee rotation angles calculated for subject 1 and subject 2 from the fluoroscopy-based (solid line) and from stereophotogrammetry (dotted line) in sit/stand and vive versa task. The arrow shows the calibration reference position. (Stagni, et al., 2005)

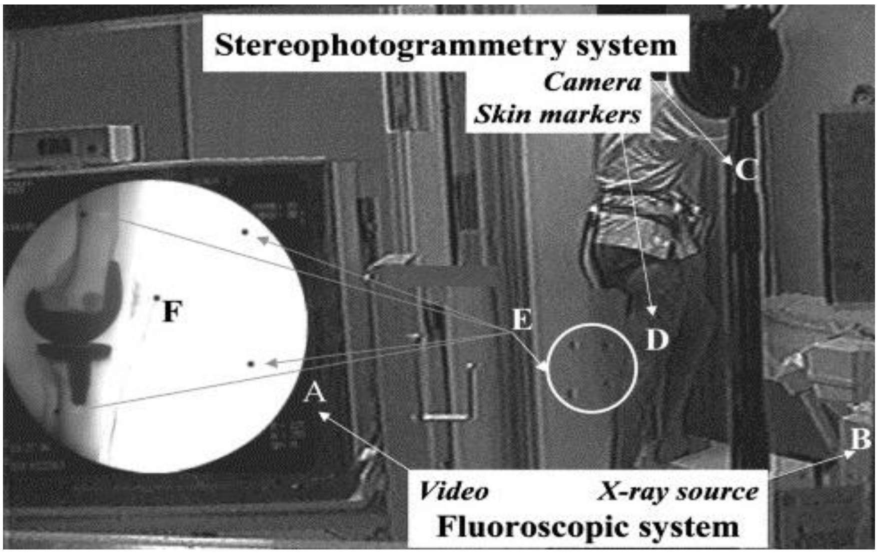

Figure 2.5 - Experimental set-up. (A) Real-time visible feed-back of the fluoroscopic images acquired. (B) X-rays source of the fluoroscope. (C) One of the five cameras of the stereophotogrammetric system. (D) Skin markers on the lateral aspect of the thigh and the shank. (E) The four specialized radiopaque/reflecting markers for spatial registration. (F) The specialized radiopaque/reflecting marker for temporal synchronization. (Stagni, et al., 2005)

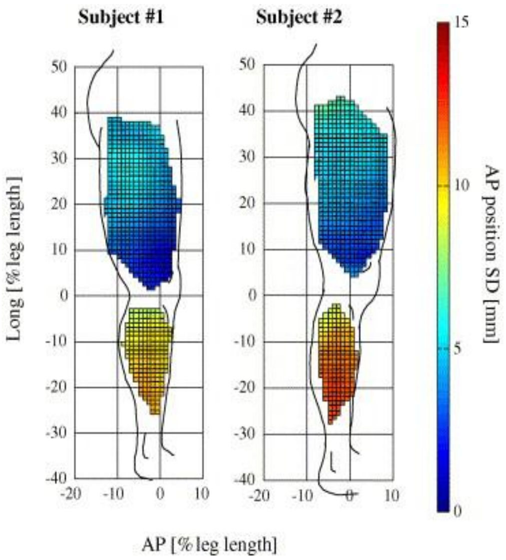

Figure 2.7 - Mapping of the standard deviation of the marker positions along the antero-posterior anatomical direction on the thigh and shank during the execution of the knee extension against gravity motor task. (Stagni, et al., 2005)

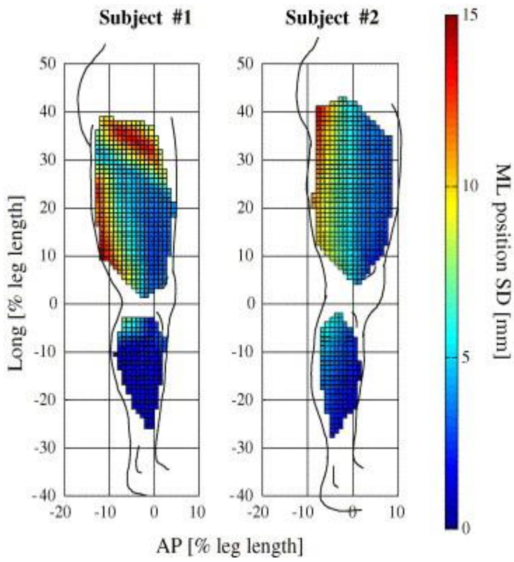

Figure 2.8 - Mapping of the standard deviation of the marker positions along the antero-posterior anatomical direction on the thigh and shank during the execution of the step up/down motor task. (Stagni, et al., 2005)

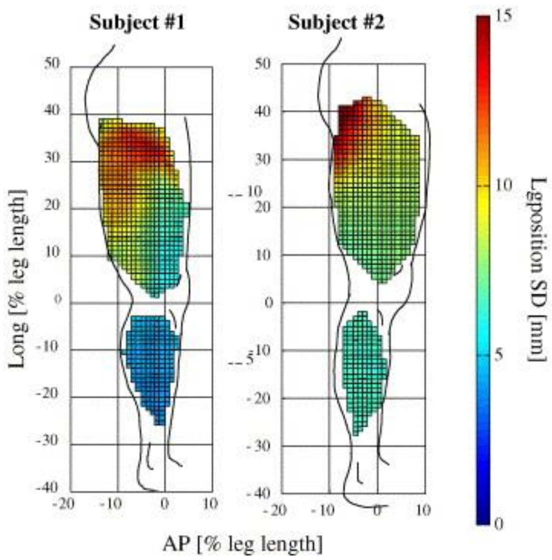

Figure 2.9 - Mapping of the standard deviation of the marker positions along the antero-posterior anatomical direction on the thigh and shank during the execution of the sit-to-stand/stand-to-sit motor task. (Stagni, et al., 2005)

Lucchetti, et al., (1998) proposed the dynamic calibration method which attempts to calibrate the anatomical landmark positions in an ad hoc motion followed by compensation with joint angles in a motor task. A study done by Ryu, et al., (2009) presented an alternative method to compensate the anatomical landmarks (AL) position by the use of a skin marker displacement rather than compensating with joint angles. In an ad hoc motion and a motor task, the technique of Lucchetti, et al., (1998) evaluates joint angles in order to model and estimate the AL displacements, respectively. It reconstructs the joint angles from the positions of anatomical landmarks that are compensated with AL displacement. But unfortunately, this method proved to be partially inefficient in continued calculation of joint angles for AL compensation because the amount of the data of skin markers and the steps involved in calculating joint angle makes the compensation procedure complex. On the other hand, the method adopted by Ryu, et al., (2009) assumes that the displacement of anatomical landmarks is related with the displacement of skin markers and attempts to model the dependency between the two. Considering that the calculation of the displacement of the skin marker is not complex, compensating AL position by skin marker displacement consumes less time and effort as compared to that with joint angles. The practicability of the projected method was tested by analysing the knee movements of a patient who was wearing an external bony fixator on the shank. As shown in figure 2.10, markers with 'M' prefix were placed on the patient's leg and the markers with prefix 'E' on the external fixator. The patient was asked to perform 3 motor tasks: a static sitting posture for anatomical calibration and 2 sets of repeated knee movements for modelling AL displacement and validating the proposed method.

Both the AL compensation methods in motion analysis procedure are significantly complex. The performance of the proposed method was compared with the Lucchetti, et al., (1998) compensation method with joint angles.

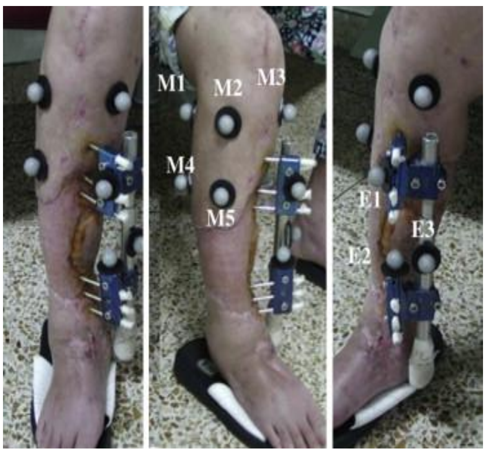

Figure 2.10 - Marker placement. (Ryu, et al., 2009)

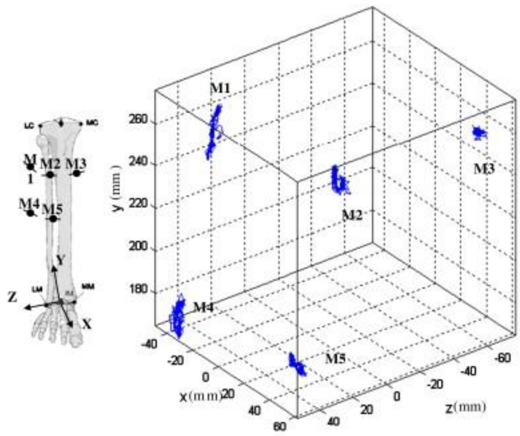

Figure 2.11 - Trajectory of skin marker displacements. (Ryu, et al., 2009)

The figure 2.11 above shows the M1-M5 skin markers displacements during motion with respect to the tibia/fibula. The proposed method proved to be efficient in reducing all the errors (rotational and translational) by 40-80% as compared to 30-70% reduction by joint angles compensation technique. Also, the errors of kinetic variables showed increased reductions of up to 25-60% by AL compensation with skin markers displacement than with joint angles. The authors conclude that the proposed method proves to be successful in minimising the STA errors and necessitate the need to validate it across various other able-bodied people.

Peters, (2010) investigated different methods to minimise STA during the measurement of kinematics and kinetics of human gait as there were no methods that were used consistently to assess STA. The main aim of the study was to find out the most valid method for minimising STA during gait analysis. It was confirmed that the STA at the tibial segment is less than for femur segment. Thus, the tibial segment of 20 unimpaired young adults was investigated for the marker locations that were least prone to STA. Out of the 36 markers on the tibia, 4 markers (distal and proximal anterior tibial crest and lateral and medial malleolar) were found to be the least susceptible to STA. The 3-D freehand ultrasound (3-DUS) was used as a new gold standard in order to assess the modelling methods. In order to ensure that the new gold standard (3-DUS) was a valid methodology, a validation of 3-DUS against MRI was done. The two imaging techniques were used for the same number of patients and 3-DUS gave the results that the distance between the left and right HJC was 4.0 $\pm$ 2.3 mm which is not much different from MRI clinically, indicating that 3-DUS can be used as a gold standard measurement for three dimensional gait analysis (3-DGA).

To validate the existing 3-DGA modelling methods, the new gold standard method was applied, in order to determine the most accurate method for HJC location. For this, 53 patients with different gait abnormalities underwent a 3-DGA along with 3-DUS of their right and left femoral heads. Data analysis was done on the 46 patients after assessing the resultant ultrasounds for image quality. For the determination of HJC, seven different methods were analysed and four out of these were investigated in two ways. The Harrington, et al., (2007) method gave the most accurate and repeatable results in which the 3-D location error was 14.3 $\pm$ 8.0mm that considerably performed better than the functional techniques. This study seems to be very useful and it highlights the importance of 3D ultrasound imaging in locating the HJC. It also claims that the predictive method performs better than functional method in locating HJC which is a contradiction to the earlier literature. This study was a PhD thesis from University of Melbourne and could not be accessed easily to look into the methodology adopted by the author. But it surely is a very useful research and the methods can be adopted for future.

Evaluation of a new algorithm by Siston & Delp, (2006) tested the accuracy of a pivoting algorithm which is used to locate the hip centre. The study lists a similar algorithm that was first given by Piazza, et al., (2004) to estimate the hip joint centre. It studied different motion patterns and their affects on the performance of the algorithm in vivo. The research by Piazza, et al., (2004), based on human kinematics, provided encouraging results but in their experiments the true location of the hip joint centre was unknown. It is thus not clear whether the errors reported by them should be attributed to the algorithm or the motion data that is collected. In general, the affects of the noise in the kinematic data on the results of different algorithms that attempt to locate the HJC are also unknown. The aim of the study by Siston, et al., (2006) was to assess the computational speed and accuracy of another algorithm called ‘‘pivoting’’ algorithm that is a modification to the one given by Piazza, et al., (2004) with restricted motion and noisy kinematic data. The study used a mechanical linkage, which meant that the exact hip centre location was known, that enabled testing the performance of the algorithm with six motion patterns and with introducing simulated noise in kinematic data. The figure 2.12 shows the mechanical linkage and its components. In the graphical representation shown in the figure R_{femur} and R_{pelvis} correspond to the reference frames on the femur and pelvis, respectively. The location of the femoral reference frame was approximately 500 mm from the ball joint.

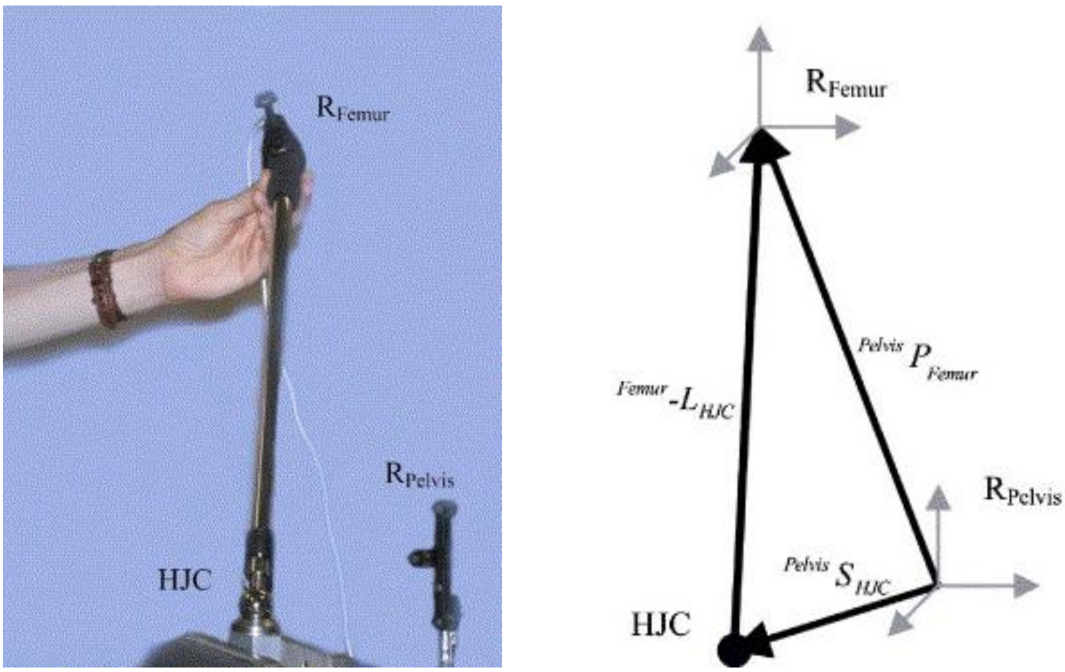

Figure 2.12 - The mechanical linkage and a graphical description of the reference frames. (Siston, et al., 2006)

The femur segment was manually rotated through six motion patterns that included single-plane and multi-plane motions. The basis for pivoting algorithm is vector addition that can be given by (Siston & Delp, 2006)

$$^{\text{Pelvis}}P_{\text{Femur,Calc}} = [^{\text{Pelvis}}_{\text{Femur}}R]^{\text{Femur}} - L_{\text{HJC}} + {}^{\text{Pelvis}}S_{\text{HJC}},$$

$^{\text{Femur}}{-L}_{\text{HJC}}$ - vector, in the femoral reference frame, originating at the HJC and terminating at the origin of the femoral frame

$^{\text{Pelvis}}S_{\text{HJC}}$ - vector, in the pelvic reference frame, beginning at the origin of the pelvic reference frame and terminating at the HJC and

$^{\text{Pelvis}}_{\text{Femur}}R$ - The rotation matrix between the pelvic and femoral reference frames that transforms $^{\text{Femur}}{-L}_{\text{HJC}}$ into the pelvic reference frame.

The algorithm was also evaluated to see how sensitive it is to noisy data by introducing varying noise amplitudes into the already calculated position of the femoral reference frame from the multi-plane motion trails. The sphere fitting algorithm from the study of Piazza, et al., (2001) was also applied to examine any variations in the two algorithms. The graphs in figure 2.13 and 2.14 show that the mean errors for multi plane motions were significantly smaller than that for single-plane motion and the mean changes in the pivoting algorithm were significantly smaller than that from sphere-fitting algorithm. The circumduction motion pattern produced the smallest mean errors of 2.2 $\pm$ 0.2 mm while the single plane motion like flexion/extension produced the largest errors of 4.2 $\pm$ 1.3 mm. The study concludes by agreeing to the superiority of the pivoting algorithm over the earlier methods for locating the hip joint centre as it is an accurate and a fast method and the algorithm is not really affected by realistic limits of motion and by the presence of noisy motion data.

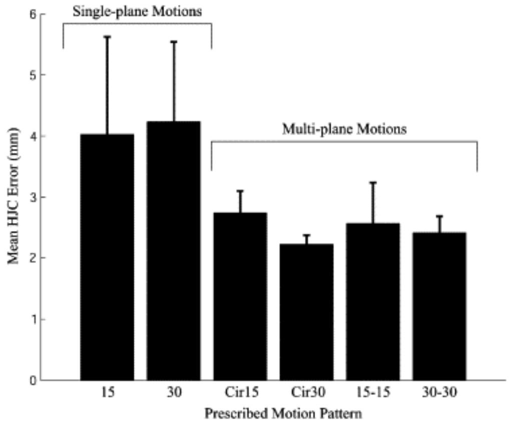

Figure 2.13 - Mean error in estimation of the HJC. (Siston, et al., 2006)

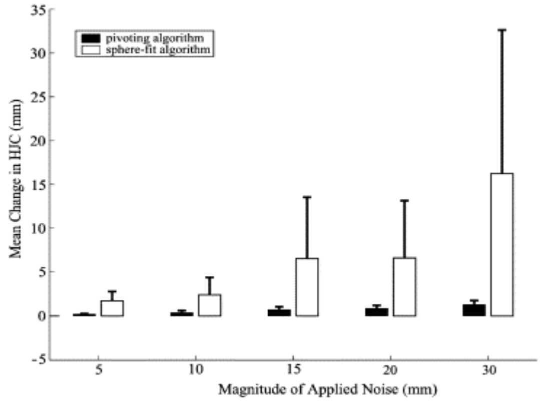

Figure 2.14 - Mean change in HJC error magnitudes with varied amplitudes of random noise with the pivoting and sphere-fitting algorithms. (Siston, et al., 2006)

2.4 IMAGING TECHNIQUES FOR DETERMINING HIP JOINT CENTRE

Ultrasound has the potential to become a gold standard for locating the HJC. Peters, et al., (2010) describes the calibration process for 3-DUS (3-D free hand ultrasound) and validates it as a potential tool of measurement for locating the HJC. This study involved creating 3-DUS images by from 2-DUS images by translating them into 3-D space with the help of the positions of the markers that are attached to the ultrasound probe and are detected by a motion analysis system. The calibration procedure adopted for this study was the Cambridge stylus method which comprises of a marker triad that defines the coordinate system and a machined rod that is has two inverse cones with a tip and is very precise as shown in the figure 2.15. The two cones form a shape that is easily recognisable in ultrasound images.

For calibration procedure, the stylus target was made to move in the water bath with the temperature of the bath maintained at 40 °C to control the speed of sound in water with temperature. The stylus target was made to move in different directions within the ultrasound image plane that resulted in a set of points which represented the position of the stylus target in that image plane. The calibration was carried out by relating the location and orientation of the ultrasound image plane in comparison to the marker coordinate system that were attached to the probe. After the calibration procedure, a marker was placed in the empty water bath and its location was determined with respect to the three markers placed on the outside that created the water bath coordinate system. The same procedure was carried out in fully filled water bath. The position of the marker determined by 3-DUS was translated into the water bath coordinate system which was then compared with its already known location.

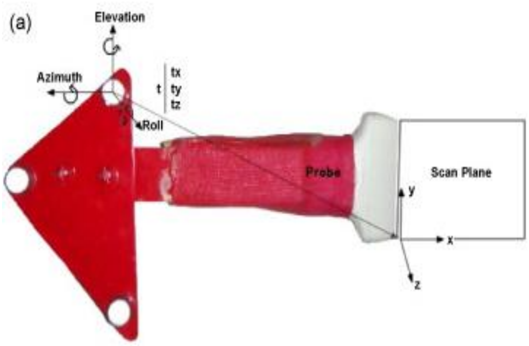

Figure 2.15 - 3-DUS Probe (Peters, et al., 2010)

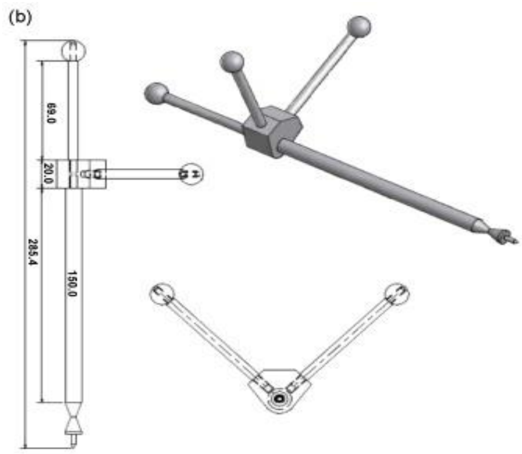

Figure 2.16 - Cambridge Stylus specifications (Peters, et al., 2010)

MRI and 3-DUS was done on twenty healthy subjects using the least squares sphere fitting (functional method) techniques like MATLAB software. The MRI scan provided data about the femoral heads and their location in 3-D by treating the data with a software application. The femoral heads were outlined and a mesh was created and exported for analysis. The location of the 3-DUS probe was determined with reference to the pelvic coordinate system and landmarks were digitised manually on the perimeter of the femoral head all over the 3-DUS images. The measure of accuracy was the inter HJC distance (distance between left and right HJC) and the radii of femoral heads because these measures did not depend on a common pelvic coordinate system.

The average difference between the inter HJC data of the two imaging techniques was 4 ± 2 mm. A box-plot of the difference between 3-DUS and MRI inter-HIC distance and radius of the femoral head showed no dependency of the variability in error on the inter-HJC distance.

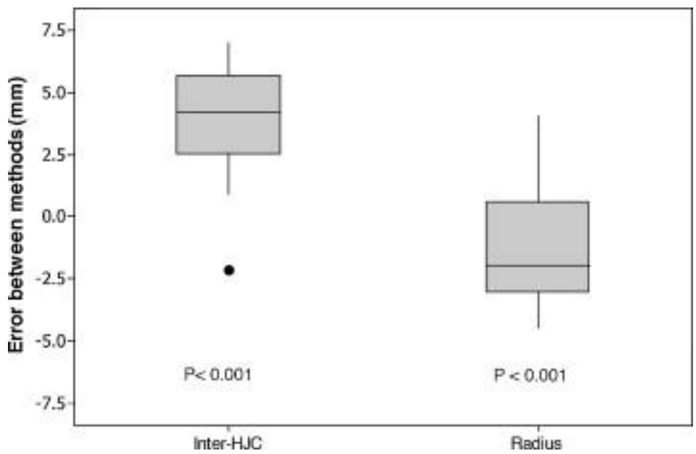

Figure 2.17 - Box-plot of the difference between 3-DUS and MRI inter-HJC distance and radius of the femoral head (● represents an outlying data point). (Peters, et al., 2010)

The minimised spread of error between 3-DUS and MRI determination of radius of femoral head shows good quality control between the two techniques. Also, this paper states a good conformity between functional and radiological techniques which indicates that the accuracy of 3-DUS is sufficiently adequate to be used for such studies validating functional calibration. The calibration error is little greater than in inter-HJC distance, suggesting that the 3-DUS is capable of identifying anatomical structures with very low errors. Thus, it can be inferred from these results that 3-DUS gives an appropriate estimate of the femoral head location supporting its use as a gold standard for 3-D gait analysis.

A study done on subjects with hip dysplasia (22 females and 4 males) aimed at calculating the femoral and acetabular cartilage thickness (Mechlenburg, et al., 2007). The study tested three stereologic methods based on MRI. The identification of the interface between femoral and acetabular cartilage was done with the help of the traction device used during MRI. The three methods gave a range of measurements for the thickness of the articular cartilage in the hip joint which was 1.15 mm to 1.46 mm for acetabular cartilage and 1.18 mm to 1.78 mm for femoral cartilage. Method 2 proved to be the least precise method as the observed total variation was the highest. The other two methods (1 and 3) gave similar results but measurements were performed on images from sagittal plane of the femoral head in method 1 and on centre images in method 3 in which the cartilage surface is cut perpendicularly and this avoids partial volume effect. Images obtained from all three methods are shown below.

This paper also lists some work done by other authors. Nakanishi et al. (2001) with MRI and traction found the cartilage thickness of the femur head to be the greatest (mean 2.8 mm) in the central portion i.e. around the ligamentum teres. The medial and lateral areas measured 1.3 mm and 1.1 mm respectively. Similarly, Nishii et al. (2004) with computational analysis of MRI showed that the mean cartilage thickness is greater in dysplastic hip, around 1.77 mm, than in normal hips, around 1.34 mm. Another cadaveric study done by McGibbon et al. (2003) used different MRI pulse sequences and revealed that the cartilage thickness ranges between 1.36 mm and 1.70 mm. Thus it is clear that all the above mentioned measurements of the cartilage thickness cannot be directly compared with the present study as these results seem to be greater than what the authors of the present study found out.

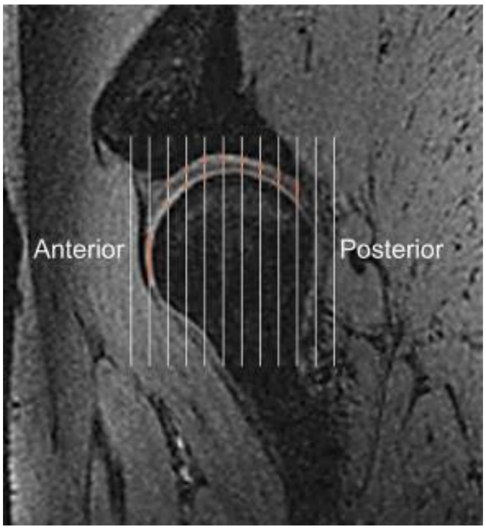

Figure 2.18 - Method 1 - Grid of vertical lines placed on the sagittal images of the hip joint and 'orthogonal' distance through the cartilage measured manually from interception of test lines and the cartilage. Mean distance/thickness was calculated from 60-80 measured distances. (Mechlenburg, et al., 2007)

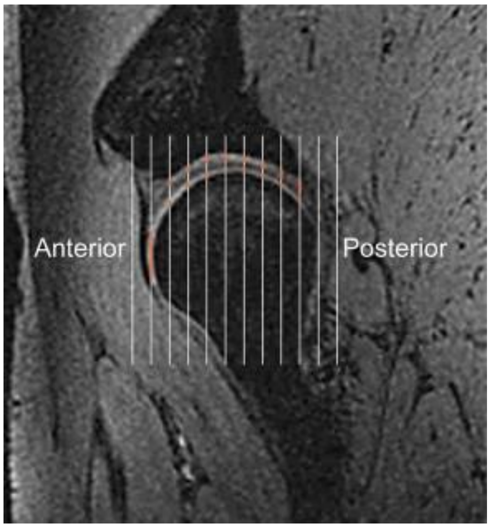

Figure 2.19 - Method 2 - Grid of vertical lines placed on the sagittal images of the hip joint and the distance through the cartilage measured manually from interception of test lines and the cartilage. Mean distance/thickness was calculated from 60-80 measured distances. (Mechlenburg, et al., 2007)

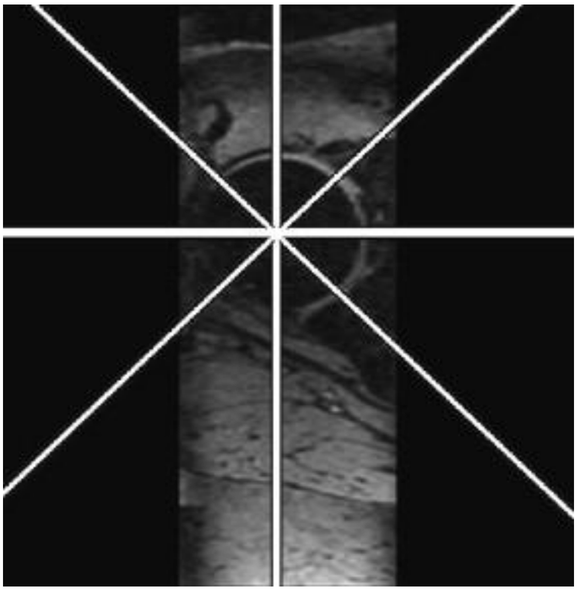

Figure 2.20 - Method 3 - Figure shows four reconstructed images consisting of a sagittal, a coronal and two images at 45° between the other two through the femoral head centre. Mean distance/thickness was calculated from 60-80 measured distances. (Mechlenburg, et al., 2007)

A study by Nötzli, et al., (2002) attempted to develop a straightforward method to define the concavity at the femoral head-neck junction. MRI was done on 39 patients with groin pain and having pathological problems and their data was compared with 35 normal control subjects. Tilted axial MR scans were done that were made to pass through the centre of the head. The angle ‘α’ was a measure of the anterior margin of the femoral neck waist and the femoral head-neck junction width was measured at two sites. Two methods were adopted for quantifying the concavity of the junction of femoral head and femoral neck. Radiologists and orthopaedic surgeons repeatedly measured the different variables independently which showed good reproducibility.

The mean angle ‘α’ seen in the figures 2.22 and 2.23 was found to measure 74.0° in patients and 42.0° in the control group. The relationship between the anterior widths of the femoral neck at two sites and the femoral head diameter (r) demonstrated considerable differences amongst the two groups. With the use of standardised MRI, it is seen that at the femoral head-neck junction, the patients with symptomatic hips having impingement have significantly less concavity than patients with normal hips. Hip impingement also called as femoroacetabular impingement is a condition in which the femoral head rubs against the acetabulum while hip flexion (McDermott, 2010).

Figure 2.21 - A coronal scout view. (Nötzli, et al., 2001)

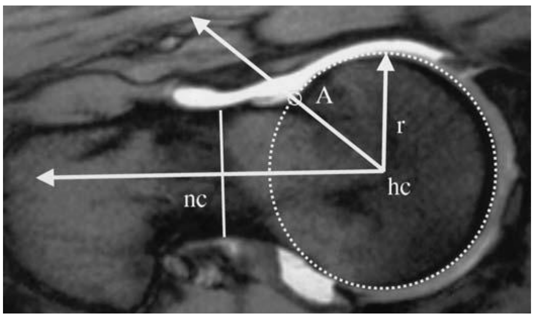

Figure 2.22. – MR images showing angle α in a normal hip (Nötzli et al. 2001)

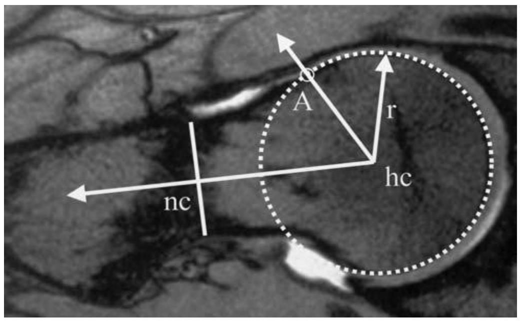

Figure 2.23 - MR images showing the angle α in a pathological hip (Nötzli et al. 2001)

There are systems that use 2D ultrasonic transducer arrays and produce 3D images in real time of a volume of interest. But these systems are costly and not easily available (The Hong Kong Polytechnic University, 2011). Yu, et al., (2011) presents a cheap system that is flexible and can integrate many components of image processing for 3D reconstruction from 2D images planes and various acoustic views. The proposed system allowed good control of the image acquisition planes for finest 3D reconstructions from numerous views. The basis of their approach was a 3D freehand ultrasound system that allowed controlling the 2D image acquisition using conventional 2D probes. They developed latest methods for image segmentation and strong multi view registration for reliable performance. Figure 2.24 shows the flowchart for software for multi-view reconstructions from 2D images. The software used was created in C language and MATLAB. It reconstructed 3D surface of the heart of a patient using segmented boundary walls with automated registration. The software measured the interference effects and allowed the use of hybrid segmentation and multi-view reconstruction with fine-scale feature based automated registration with the help of a non-linear least squares algorithm. Figure 2.25 lists the multi-view registration algorithm. It uses a 3D Hotelling transform which performs initial registration and provides early estimates for optimal parameters which are found afterwards using non-linear least squares. The design of a 3D freehand ultrasound system built from 2D machine discussed in the paper allows expert control over the acquisition geometry. A calibration was performed in order to determine the spatial relationship between the sensor and the 2D images for accurate 3D reconstructions.

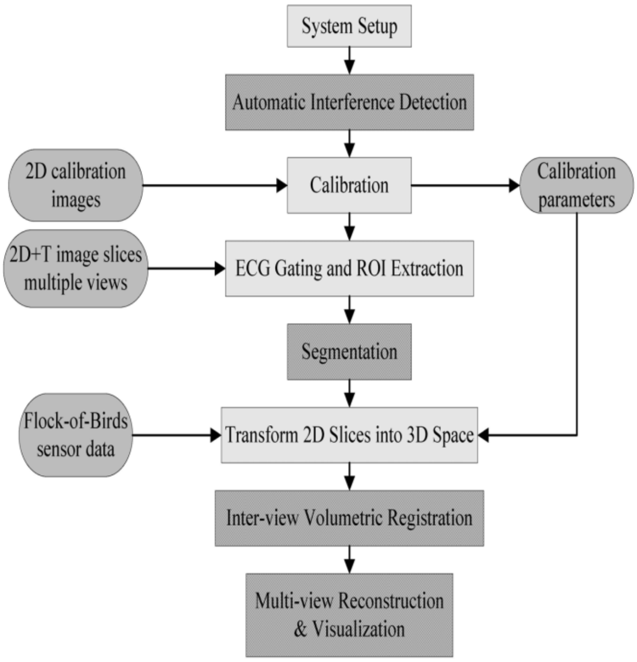

Figure 2.24 - Software flowchart (Yu, et al., 2011)

1. ***Perform segmentation to estimate object wall boundary in individual 2D image slices.***
2. ***For the segmented object, construct a thin wall surface boundary using the set difference of the binarized object with an eroded version of the object.***
3. ***Select the full-sweep view as the reference view. For each view, perform 3D volumetric reconstructions of the wall surfaces using tessellation-based, linear interpolation.***
4. ***Apply a 3D Hotelling transformation to center each view to the coordinate origin and the principal axes of the reference view.***
5. ***Transform all non-reference views to the reference view and compute the mean square error.***
6. ***Use robust non-linear least squares (Levenberg-Marquardt) to obtain optimal registration parameters.***

Figure 2.25 - Multi-view registration algorithm. (Yu, et al., 2011)

Results showed that measured error of volume of multi-view reconstruction was less than 5% of the true volume. For in-vivo cardiac experiments, from multi-view 3D reconstruction volume measurements of the left ventricle was found to be consistently and significantly in better conformity with clinical measures than measurements from single-view reconstruction. These results led to the conclusion of multi-view 3D reconstruction from limited 2D freehand images being more exact in volume quantification as compared to systems with single-view reconstruction.

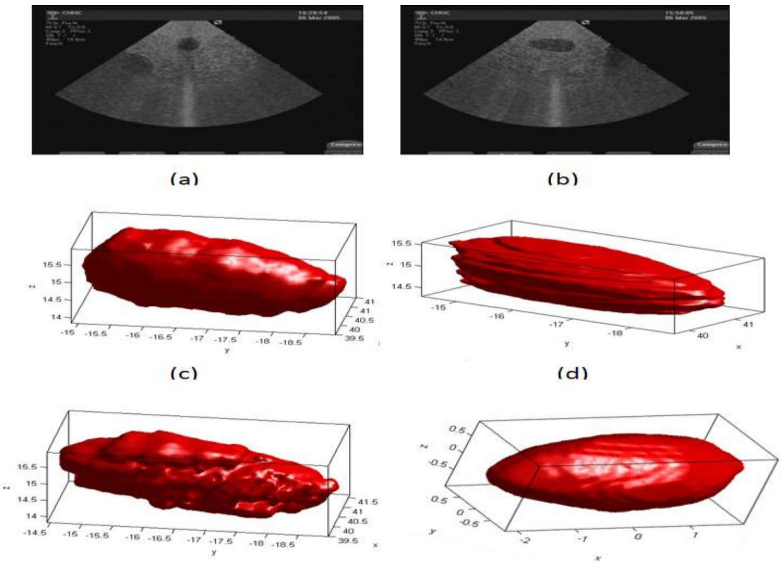

Figure 2.26 - Multi-view (single and 2-view) reconstruction with registration for the calibrated phantom
(Yu, et al., 2011)

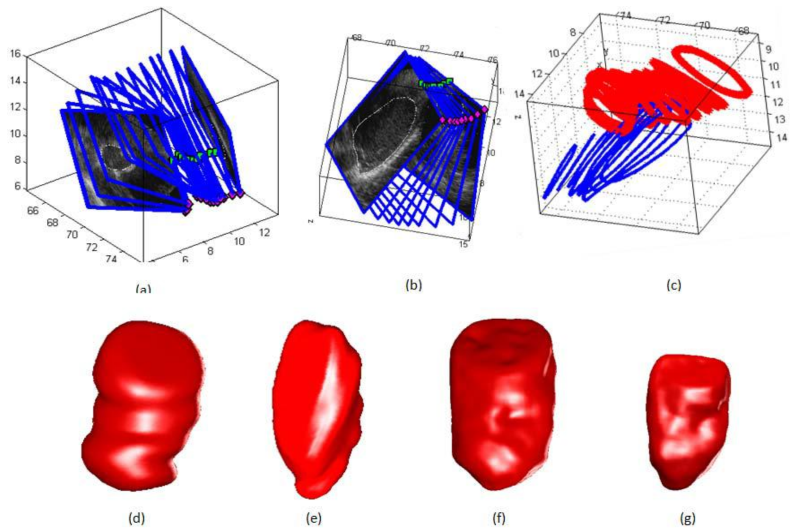

Figure 2.27 - Two view 3D reconstruction using in-vivo cardiac images (Yu, et al., 2011)

CHAPTER 3.

METHODOLOGY

3.1 BACKGROUND

There have been many studies that aim at locating the hip joint centre accurately. A number of methods have been developed to know the coordinates of the HJC. But none provides results that give the exact location of the HJC. The methodology adopted in this study is adopted from Simpson, (2011). He assessed the accuracy of predictive and functional methods through various validation techniques (MRI, Ultrasound) that provided reasonable results for analysis. The predictive methods as said earlier provide the regression equations that are based on pelvic depth, width and length of a subject (Harrington, et al., 2007). But for these equations, there are certain assumptions made that are unlikely to occur in practice. These equations assume that the pelvis is symmetric and thus a great deal of errors is seen due to differences in pelvic geometry in different individuals.

The functional methods in spite of being more accurate than predictive methods suffer from various other problems. The functional method adopted is the sphere fit method that works on a principal which states that if a limb is to be circumducted then all the points on the limb will be lying on the surface of corresponding spheres that share common centre of rotation (Gamage & Lasenby, 2002). In this case, it is the Hip Joint Centre. The problem with this method is that the results obtained by this method are affected by significant amount of skin tissue artefacts. These arise while the circumduction of the leg is performed.

In this study, some of earlier results by Simpson, (2011) are reviewed to fill in some unknown data like the actual measurements of the model which were not included in his study. The mechanical model is analysed in more detail which is explained further. Ultrasound is better explored. Also, possible methods have been adopted to minimise the skin tissue artefacts.

3.2 CHOICE OF ALGORITHM – MATLAB PROGRAM

The functional method that is used to create the algorithm is the Gamage and Lasenby method. This method was developed in 2002 that involved using the position of markers to determine the HJC location. It works on the principle that a vector set on a body rotates around an axis of rotation that is varying in time with the set centre of rotation and with the vector tips lying on concentric spheres. This requires a frame rate to be selected, thus the marker positions are recorded accordingly. It selects the individual marker trajectory and applies a method (*least squares*) between the marker trajectory radius and the distance of each marker from the HJC (Gamage & Lasenby, 2002).

A MATLAB program based on the above algorithm is used to process the data captured from VICON system. The program used the data collected from the mechanical model to validate the algorithm. A local coordinate system was developed using the four hip markers and the trajectories from the leg markers were then transferred into this new system. The MATLAB program determines the relative position of these markers to the HJC in the form of coordinates. The program then gives a centre of rotation that is common to all points throughout the markers' trajectories. It then finally gives an output of the predicted coordinates for HJC in relation to the local coordinate system origin (first hip marker). For subject testing, the axis system defined by Wu, et al., (2002) is adopted. The MATLAB code for the mechanical model as well as subject testing can be found in the Appendix.

3.3 MOTION ANALYSIS SYSTEM – VICON NEXUS

There exist a number of gait analysis systems that are used in many industries including the medical field. These systems allow the user to record number of parameters including the kinetic and kinematic data of a subject. These systems have been a great benefit in medical field and have proved very useful in detection of human activity like motion analysis of body parts. The VICON system used in this study tracks the position of infra-red reflective markers in space via 12 cameras placed all over the laboratory. This is achieved when each camera records the location of the markers in a 2D plane view by detecting the reflected signals from the markers. The location and number of cameras makes it possible to combine the data from each camera and generate a 3D view in space of the marker's location with a very little error. There are different sizes of markers available. Smaller the marker, smaller is the corresponding volume that is accurately captured.

The VICON system requires static and dynamic calibration each time it is switched on. This is not a necessity but it is recommended to calibrate it each time before one starts using it in order to get accurate results. The calibration wand shown in the figure 3.1 has 5 small markers on it which is waved around the working space until all the cameras obtain sufficient amount of information. The process is finished when a small blue light on each camera stops blinking. This enables the system to verify the location of each camera. After the dynamic calibration, the static calibration is also performed with the same wand by placing it in the middle of the room. This placement allows the system to mark the origin of the global coordinate system.

The system comes with tracking and reconstruction software called Nexus software package that allows the user to create user-defined applications. These applications include marking and labelling each marker and recording each marker trajectories over time. The figure 3.1 below shows the layout of the workspace in top and front view with the cameras shown in green.

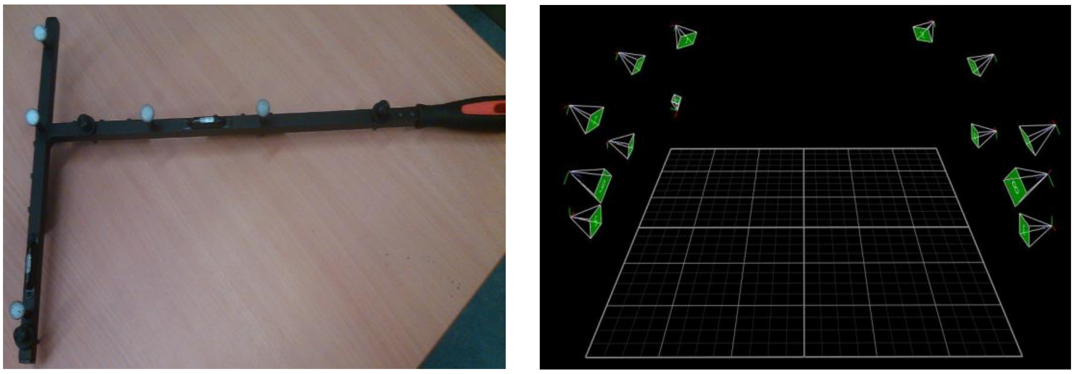

Figure 3.1 – Wand showing the markers placement and VICON lab layout as seen on the screen

3.4 DATA ACQUISITION BY VICON SYSTEM

The VICON motion capture system described in the above section was used to perform tests on the mechanical model as well as human subject and obtain data via the Nexus software (also described in the above section). The user-defined applications in the software allows to export the collected data as a .csv file which is an excel file format. This file contains all the markers' trajectories in x,y,z directions over the number of frames collected.

3.4.1. MECHANICAL MODEL TESTING

The mechanical model was the one that was used for the last year's project consisting of a hip joint connected to a metal rod with metallic pins projecting from it at different angles and locations. These pins were used to place the markers at a distance from the rod. There were 4 hip markers and 4 leg markers placed on the model that was attached to a stand for stabilization as shown in the figure 3.2. After its static calibration, sets of dynamic data were collected by performing the circumduction of the leg. The trajectories of the markers were recorded and used to validate the algorithm for the study.

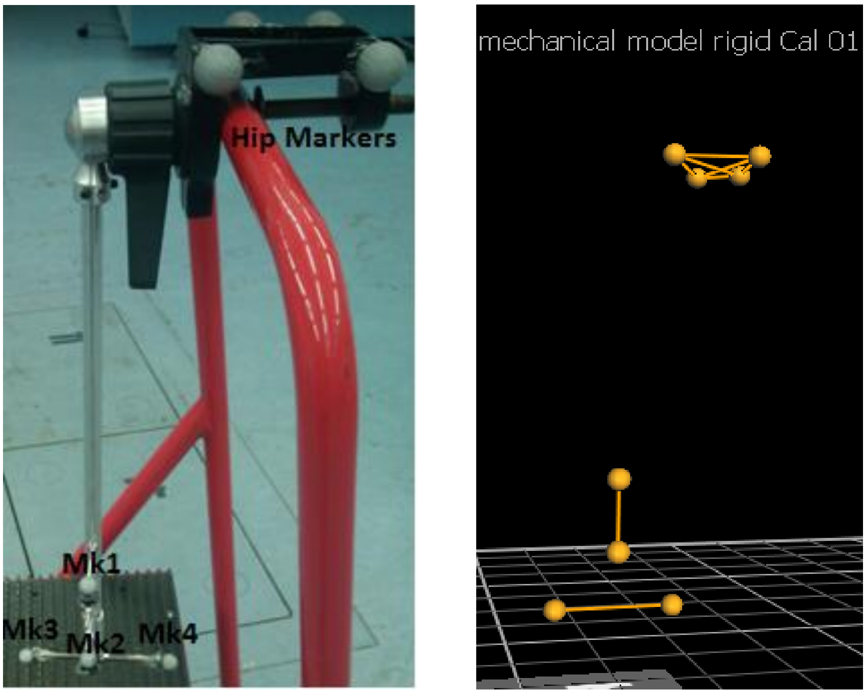

Figure 3.2 - Mechanical Model on the stand and Nexus Screenshot showing hip and thigh markers.

The actual dimensions and position of the ball segment of the mechanical model was also of interest. But it was not possible to measure it with measuring tools because the upper surface of the ball is cut which makes it an incomplete sphere. Thus, 2 additional markers were placed on the socket of the ball at a distance Y1 = $\sqrt{(r^2 + \frac{x^2}{4})}$, where 'r' is the radius of the ball and 'x' is the diameter of the cut surface of the ball. The markers were placed such that the line joining the two markers passes through the diameter of the ball. The distance Y1 is calculated from the anterior diameter of the socket that is visible in figure 3.3. Next, the circumduction was performed and the trajectories were recorded for use in the algorithm. The VICON screenshots for the two models are shown in the picture.

The dimensions of the rod (from the top of the ball) and the positions of the markers from the ball segment are shown in the figure 3.4.

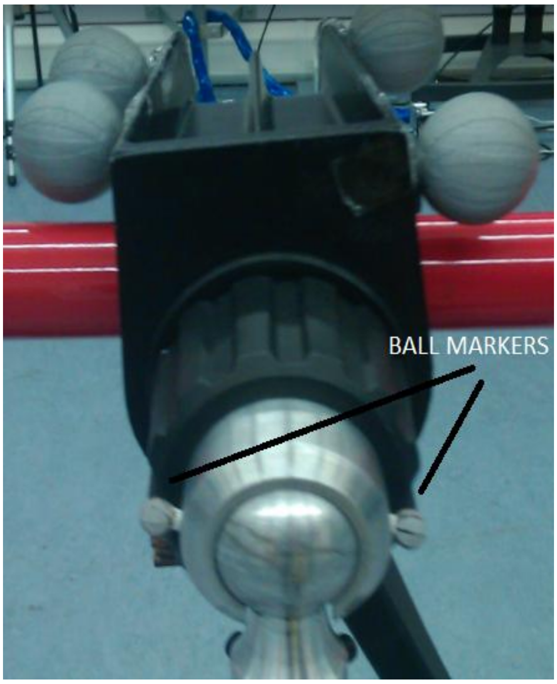

Figure 3.3 - The two ball markers on the socket

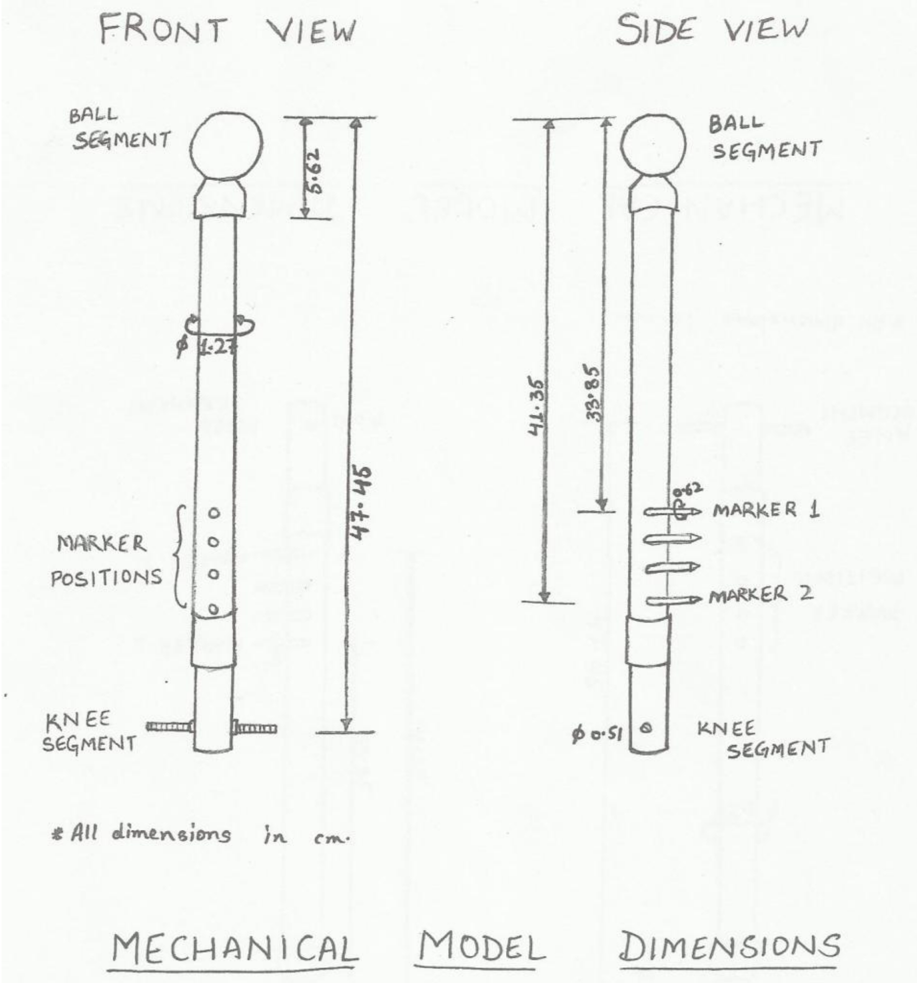

Figure 3.4 - Mechanical Model Dimensions

3.4.2. SUBJECT TESTING

Similar to Simpson's (2011) study, a local coordinate system was made by positioning the markers on the subject's bony landmarks of the pelvis which have fairly less artefacts. The bony landmarks of the pelvis are Anterior Superior Iliac Spine (ASIS) and Posterior Superior Iliac Spine (PSIS) on both left and right sides (Wu, et al., 2002). The subject testing was affected by the skin tissue artefacts, thus in addition to choosing the coordinate system which is least affected by artefacts; subjects with less fatty tissue were preferred so that the artefacts due to the amount of movement of the tissue over the thigh could be minimised. Subject 1 is a 25 year old female weighing 52 kilos and having a height of 166 cm and subject 2 is a 23 year old male weighing 80 kilos and having a height of 188 cm.

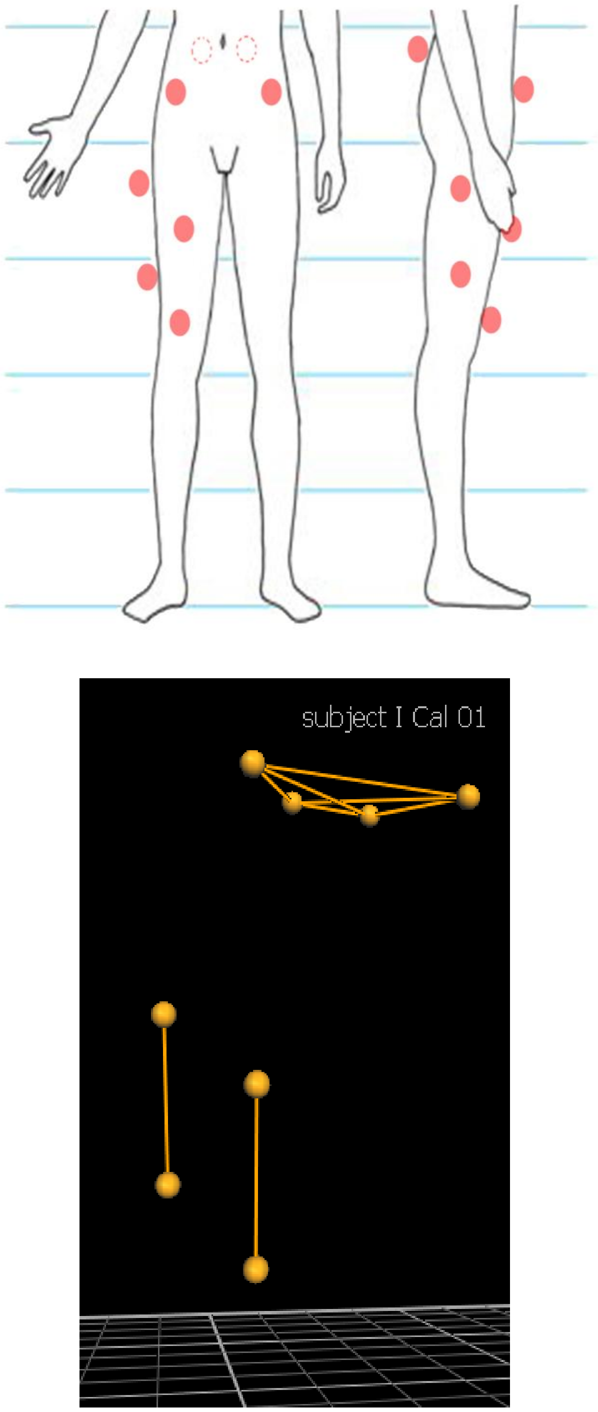

Figure 3.5 - Subject 1 marker positions (Simpson, 2011) and Nexus screenshot

The marker positions also decide the amount of skin tissue artefact in the subject testing. Thus, 8 markers were positioned on both the subjects with different orientation. For subject 1, as shown in figure 3.5, 4 markers were placed on each Anterior and Superior Iliac Spine, 2 anteriorly on the thigh and 2 laterally. The other figure also shows the VICON screenshot during subject 1 testing with the markers shown in small yellow spheres.

Once the markers were attached and secured properly, subject 1 was made to stand in the centre of the laboratory to carry out a static calibration and label the markers to generate appropriate segments. The 8 markers were labelled as ASIS right, ASIS left, PSIS right, PSIS left, Thigh anterior 1, Thigh anterior 2, Thigh lateral 1, thigh lateral 2. Similar to the mechanical leg, subject 1 performed circumduction of the leg and all the 8 markers and their trajectories were tracked through the VICON system. The coordinates of all the markers were recorded and analysed in MATLAB.

For subject 2, the position of the leg markers was changed. Subject 2 was the same subject used last year for Simpson’s (2011) study. Hence, the position of markers was changed in order to evaluate and compare the data obtained in this study with last year’s data. There were 4 markers on the hip similar to subject 1and 4 on the knee region – one on the patella, one on the tibial tuberosity and 2 on the femoral epicondyles on either side of the knee. The positions of the knee markers were chosen such that they had the least skin tissue movement. The subject 2 was asked to circumduct the leg without flexing the knee. The trajectories obtained through the VICON system were analysed in MATLAB. The position of the markers for subject 2 is shown in the figure 3.6.

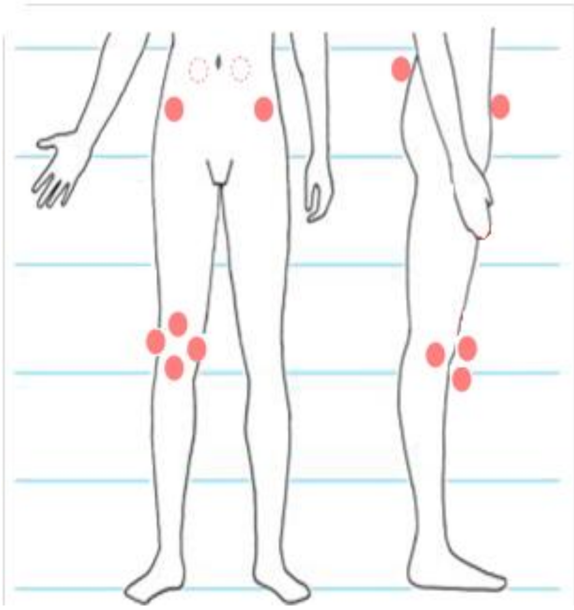

Figure 3.6 - Subject 2 marker position

3.4.3. ULTRASOUND IMAGING

As mentioned earlier in chapter 2, 3DUS is considered a new gold standard measurement for three dimensional gait analysis (3-DGA). But the ultrasound machine that was available for testing was a Toshiba - Just Vision 400 which does not have 3D feature in it. Besides that, it is a good machine for ultrasonic imaging. Simpson, (2011) also used the same equipment. But his technique was not very precise. His method involved positioning the transducer horizontally on the anterior surface of the thigh and placing the markers manually with ink on the skin surface; one at ASIS and second at the point where the probe gives the image of femoral head on the screen. Markers were also placed on the screen indicating the distance between the skin surface below the probe and the femoral head. Thus, the 2 coordinates (y, z) were calculated from the markers on the skin with ink and the 3rd (x) from the screen.

This method was not very accurate because there were significant amount of errors in it. Thus, the goal was to explore other methods that use ultrasound to image the hip joint. As described earlier in section 2.4, the technique of converting 2D ultrasound images into 3D is expensive and not easily accessible, thus due to time constraints and the above mentioned reasons, only 2D images were collected using a connector along with frame grabber software that allows capturing the real-time image from the machine to the computer. This software allows to record and store snapshots and videos and processes them as desired. Besides the software, the probe movement also plays an important role. Ultrasound testing was done on subject 1. The probe used was a phased array transducer. The subject was in standing position and the probe was moved from anterior to lateral part of thigh over an angle of 90° capturing images of the femoral head from various angles via the frame grabber into a computer. The images that were obtained are shown in the figure.

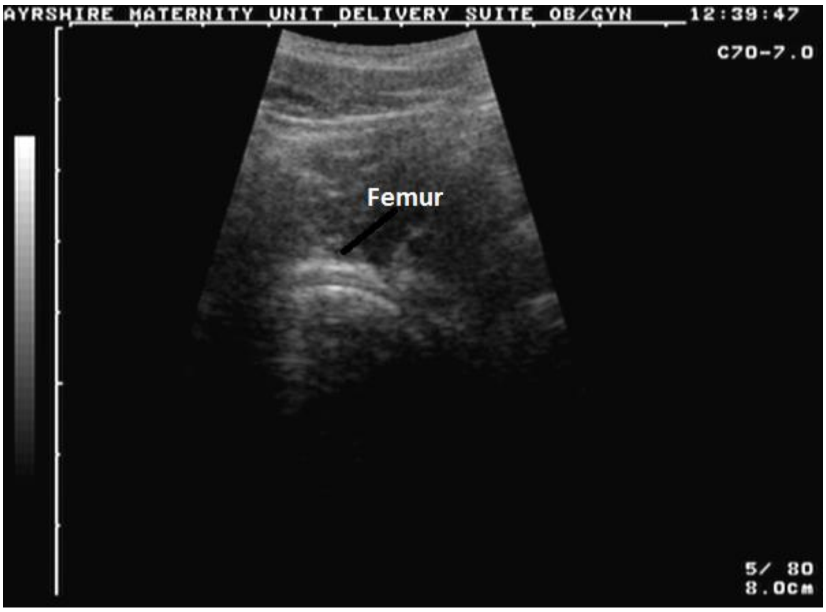

Figure 3.7 – 2D Ultrasound image of femur head of subject 1

3.4.4. PREDICTIVE VALIDATION

Harrington, et al., (2007) gives a set of regression equations that are used in this study to validate the functional testing data with a predictive method. It is important to validate these results because the predictive methods remain the most popular technique to locate the HJC in clinical settings. Many studies claim that these equations yield most accurate results for predictive methods. MRI has been used to validate them. The equations produce the coordinates of HJC and are given as follows (Harrington, et al., 2007):

$$X = -0.24PD-9.9$$

$$Y = -0.30PW-10.9$$

$$Z = 0.33PW+7.3$$

Where PD is pelvic depth and PW is pelvic width. Thus, the Nexus data was used to compute the x, y and z coordinates of the HJC by predictive method. This validation enables to determine whether the predictions are correct or not.

3.4.5. MRI VALIDATION

The MRI is known to be the best form of validation technique. But it is not very easy to perform a MRI test due to the high cost factor. Thus, the MRI data from Simpson's study was included in this study. MRI has been proved to be a very useful imaging technique that provides very accurate location of the HJC. For a MRI scan, it is important to establish a correct coordinate system and to achieve this, capsules made of cod liver oil were used and placed on the pelvic landmarks of the subject. This formed the same coordinate system that was used in VICON subject testing. This allowed better comparison of various results from different methods as the local coordinate system is kept same throughout all validation techniques. This was how the MRI test was performed last year and it gave fairly accurate results.

The MRI test that was carried out last year by Simpson used a GE Medical Systems Signa 3.0T scanner. The field of view was set at 350mm to include larger scanning area incorporating both pelvic bony landmarks and the femur head. High resolution was achieved by taking 126 slices at 2.5 mm increments. After the data was collected from the scanner, it was uploaded into software known as Mimics which allows detecting the bony landmarks and their analogous distances (Simpson, 2011).

CHAPTER 4.

RESULTS & DISCUSSION

4.1. MECHANICAL MODEL RESULTS

4.1.1. TRIAL 1

The mechanical model trial 1 was used to test the MATLAB algorithm that was created on the functional method proposed by Gamage & Lasenby (2002). The marker positions on the thigh segment were the same as used by Simpson, (2011) in his study. This trial was performed in order to repeat Simpson's experiment and to relate it to his results. The results from the algorithm gave the computed coordinates of the centre of rotation (C) relative to the hip markers, radii for all the thigh markers (Mk 1 - 4) and four hip marker trajectories (figure 3.2). The results obtained are:

$$C = \begin{bmatrix} -51.71 \\ -44.26 \\ 58.73 \end{bmatrix} \text{mm}$$

Mk1 = 314.8475

Mk2 = 391.9312

Mk3 = 467.3859

Mk4 = 464.1255

It was intended to position the marker 3 and 4 (figure 3.2) at equal distance from the centre of the rod but the variation in radii of both the markers show that even a slight error has significant effect on the final outcome of the test. Figure shows the hip and thigh tracks plotted in Global and Local Coordinate System. The individual trajectories are clearly visible which ensures that the data was correctly exported from Nexus software.

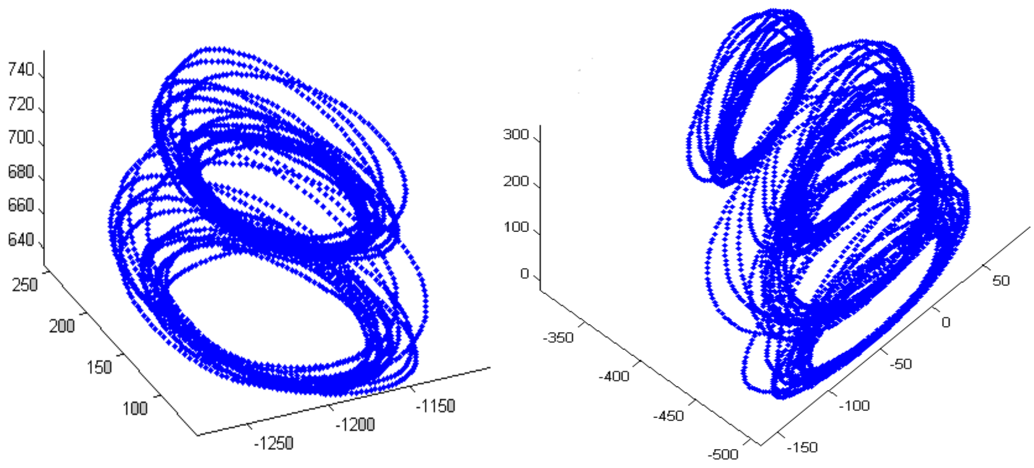

Figure 4.1 - Trajectories of thigh and hip markers in Global Coordinate System and Local Coordinate System

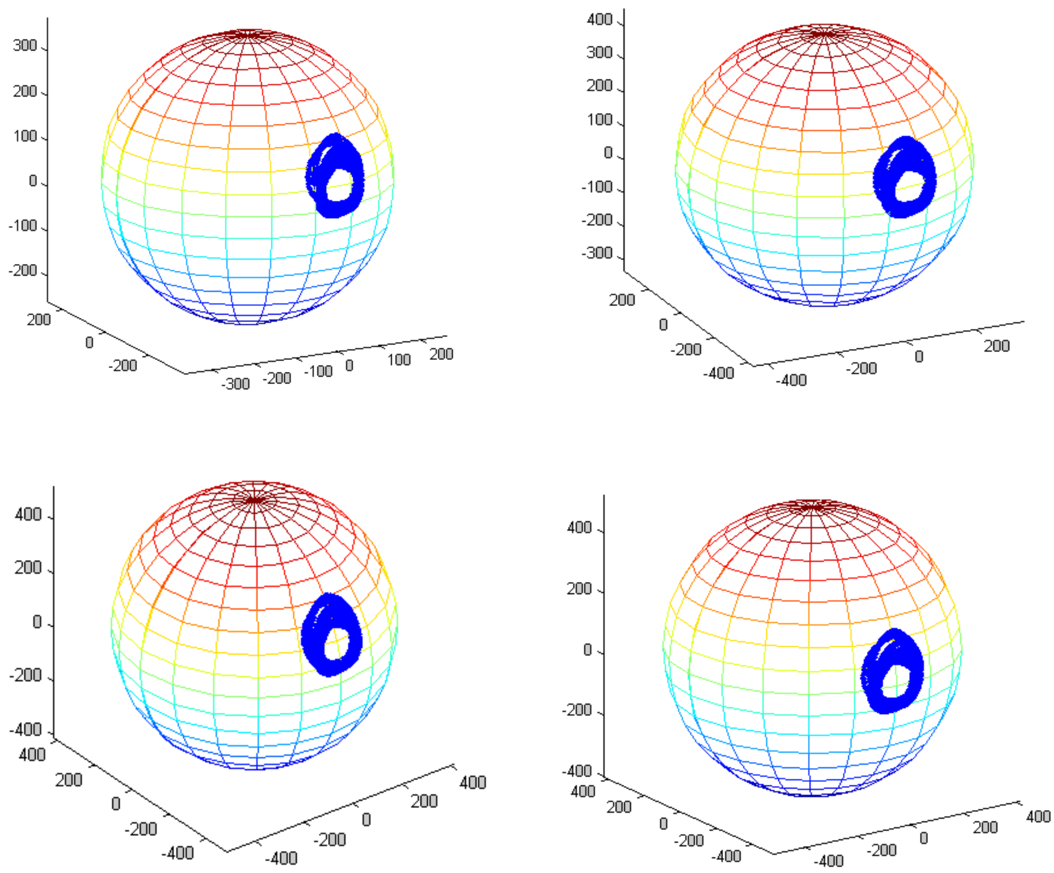

Figure 4.2 - Trajectories of thigh markers on their corresponding spheres in Local Coordinate System

The figure 4.2 shows individual marker trajectory (blue circles) on its individual sphere where each sphere has a common centre of rotation. Each individual marker was found to have a bias of an order of 10^{-5} and *root mean square error* of 0.23 mm or less. A similar experiment was performed by Cereatti, et al., (2009) with reduction in STA by using intercostal pins who reported values of *rms* error less than 0.3 mm. Present study results compare well with their study. This indicates that the algorithm works well and can be used further for analysing subject data.

4.1.2. TRIAL 2

The trial 2 was performed in order to estimate the centre of rotation from the ball markers and compare the results with that given by Gamage and Lasenby (2002). The centre of rotation estimated from the ball markers (C_b) and radii of the thigh markers (Mk_b 1 - 4) from the ball markers were found to be:

$$C_b = \begin{bmatrix} -53.28 \\ -44.15 \\ 63.27 \end{bmatrix} \text{mm}$$

$$Mk_b\,1 = 335.09$$

$$Mk_b\,2 = 406.18$$

$$Mk_b\,3 = 464.40$$

$$Mk_b\,4 = 462.64$$

The centre of rotation (C) with respect to hip markers estimated by Gamage and Lasenby (2002) was found to be as follows:

$$C = \begin{bmatrix} -53.82 \\ -43.84 \\ 62.35 \end{bmatrix} \text{mm}$$

The radii of the thigh markers (Mk 1 - 5) estimated by Gamage and Lasenby (2002) are:

Mk1 = 335.82

Mk 2 = 406.87

Mk 3 = 465.04

Mk 4 = 463.12

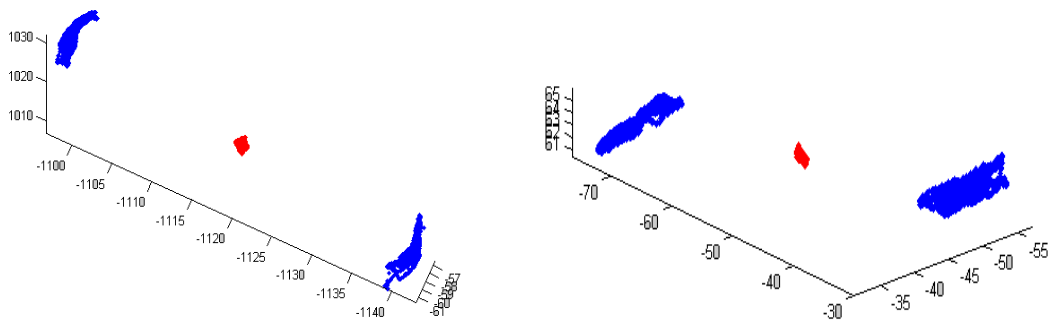

Figure 4.3 - Trajectories of ball markers in Global and Local Coordinate System

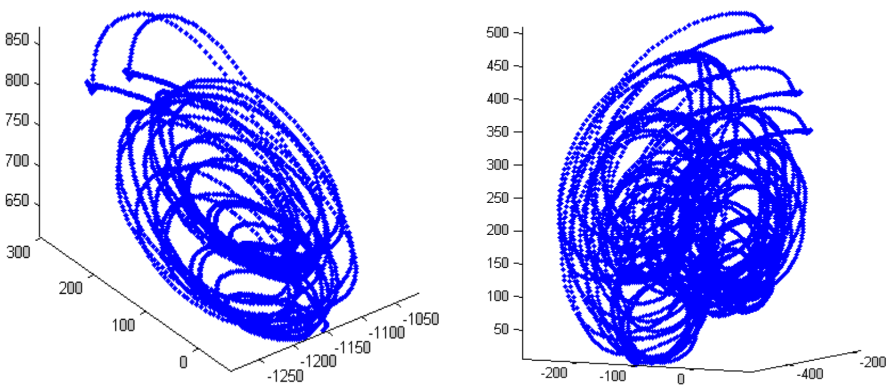

Figure 4.4 - Trajectories of thigh markers in Global and Local Coordinate System

The figures above show trajectories of ball markers and hip and thigh markers in Global and Local reference systems. The accuracy of the coordinates of the centre of rotation is on the scale of 1 – 2 mm which is quite a good estimation of the centre. Also, from the above results it is seen that the difference in the estimation of the centre of rotation (C_b - C) and radii of the markers (Mk_b - Mk) by the two methods is quite small and is as follows:

$$C_b - C = \begin{bmatrix} 0.54 \\ -0.31 \\ 0.92 \end{bmatrix} \text{mm}$$

$$Mk_b - Mk\ (1 - 4) = \quad -0.7235 \quad -0.6961 \quad -0.6348 \quad -0.4796$$

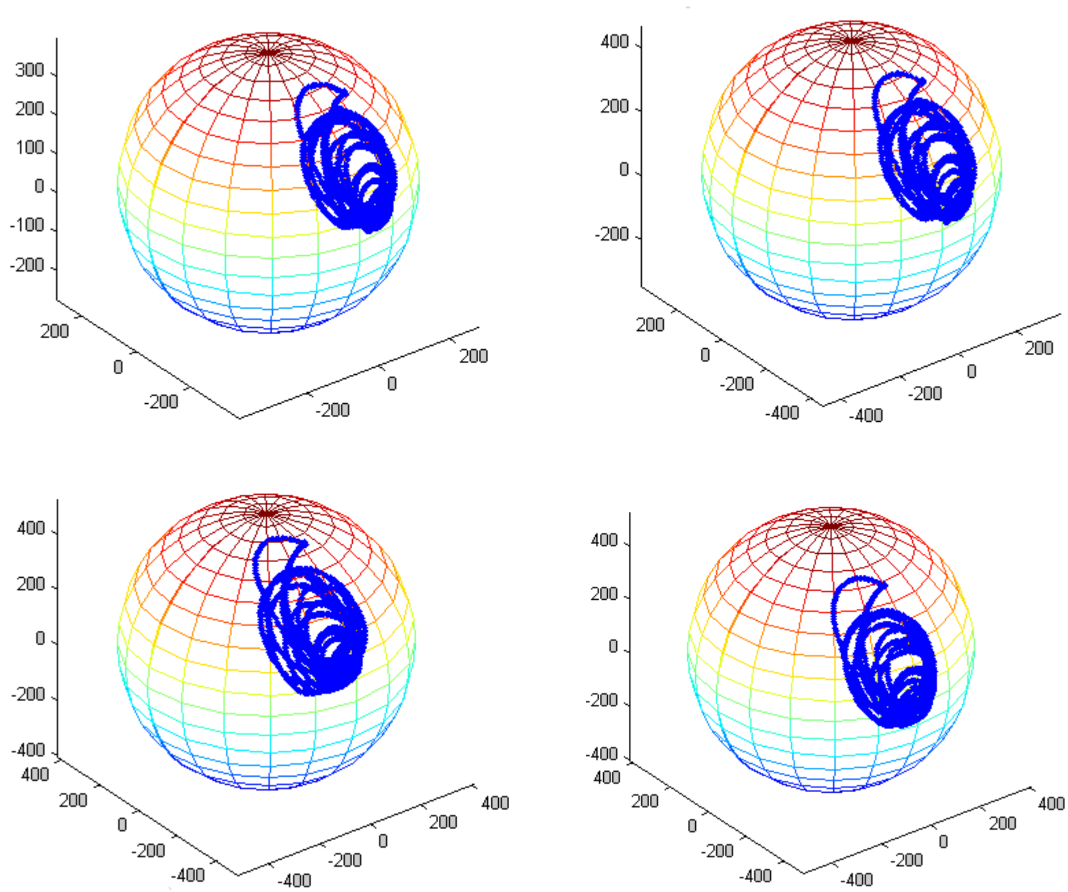

Figure 4.5 - Trajectories of the thigh markers on their corresponding spheres in Local Coordinate System

Figure 4.5 shows thigh marker trajectories on their respective spheres in Local Coordinate System. The results for centre of rotation and radii of the markers obtained by ball markers in Trial 2 for mechanical model showed good correlation with the results from Gamage and Lasenby (2002) algorithm which can be seen in the differences computed above for both methods. This was achieved by trying to fill up gaps and accommodate all the points in larger circles. This can be observed in figure 4.4. The right figure shows more dense trajectories with fewer amounts of gaps between them than in the left one. Circumducting the mechanical model in spiral manner helped to achieve the above results.

4.2. SUBJECT TESTING RESULTS

The MATLAB after doing well with the mechanical model was applied to subject data. The Local Coordinate System used was same as the mechanical model because similar to the mechanical model, 4 hip markers were placed on the each subject's bony landmarks on pelvis. Wu (2002) describes the Local Coordinate System with the axes being orthogonal which however might not be possible in practice due to the structure of the pelvis during subject testing. Thus, the algorithm was changed accordingly to yield orthogonalized results. Wu (2002) also positioned the origin of the Local Coordinate System at the right ASIS instead of locating at centre of the pelvis. Thus, all the results are orthogonalized with respect to ASIS as origin.

4.2.1. SUBJECT 1

For the subject data, the thigh markers radii were averaged over the entire trajectory. The centre of rotation and radii for subject 1 was obtained as:

$$C = \begin{bmatrix} -45.00 \\ -103.03 \\ -21.25 \end{bmatrix} \text{mm}$$

Mk 1 = 212.1252

Mk 2 = 364.5700

Mk 3 = 165.3725

Mk 4 = 300.7681

The differences between the maximum and minimum radii were observed as:

ave_dist	min_dist	max_dist
212.1238	210.1301	214.4794
364.5681	360.8119	367.4435
165.3689	161.6372	168.0075
300.7667	298.0941	303.1972

On closer examination, it is seen that markers 2 and 3 experienced largest differences between the maximum and minimum radii of 6.63 mm and 6.37 mm respectively. Marker 2 was positioned anteriorly on the thigh closer to the knee and marker 3 was positioned laterally away from the knee. The difference shows that these 2 markers were clearly more affected by STA, perhaps there was more movement of the skin tissue at these locations. The marker trajectories are shown in the figure below.

The figure 4.6 similar to the mechanical model shows the 4 thigh markers' trajectories in global and local coordinate system. The first figure has only few tracks plotted in the global coordinate system just to provide clarity.

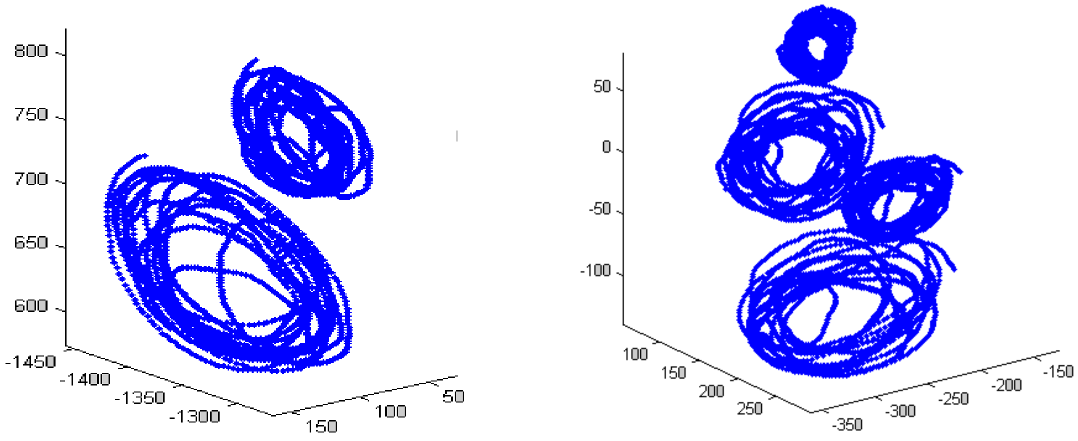

Figure 4.6 - Trajectories of thigh markers in Global and Local Coordinate System.

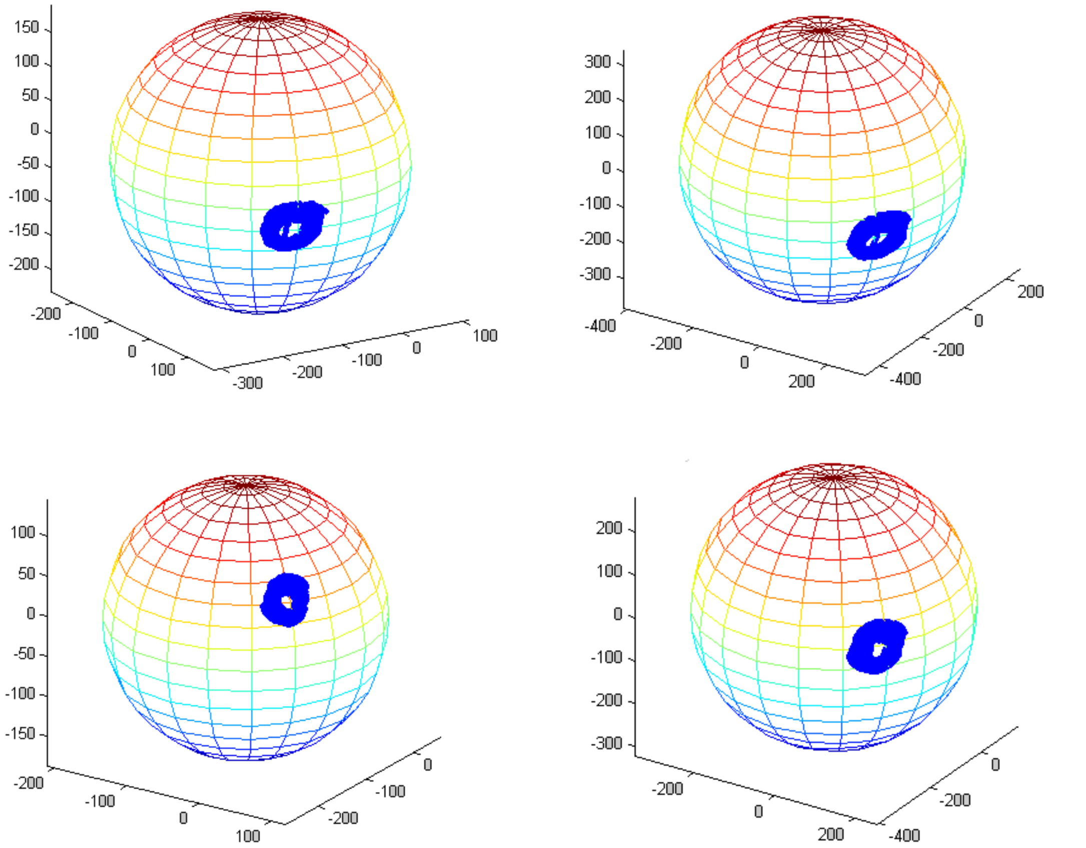

Figure 4.7 - Trajectories of thigh markers on their corresponding spheres in Local Coordinate System

Figure 4.7 resembles that of mechanical model, displaying thigh marker trajectories on their respective spheres, each with the same centre of rotation.

4.2.2. SUBJECT 2

As said earlier, subject 2 for the present study was the subject 1 from Simpson's (2011) study. So the data obtained for subject 2 is comparable with the last year's results. The centre and radii were obtained as follows:

$$C = \begin{bmatrix} -55.02 \\ -97.35 \\ -19.85 \end{bmatrix} \text{mm}$$

Mk1 = 444.17

Mk 2 = 503.15

Mk 3 = 443.41

Mk 4 = 444.45

The differences between the maximum and minimum radii were found to be:

ave_dist	min_dist	max_dist
444.1461	436.9321	467.5151
503.1410	494.1392	514.7270
443.4032	437.5906	457.0327
444.4431	438.4450	457.9323

Examining the results closely, it can be seen that the markers 1 and 2 experience largest amount of STA with the difference in their maximum and minimum radii as 30.58 mm and 20.58 mm. These markers were positioned on the patella and tibial tuberosity respectively. These two positions are known to have least skin movements but unfortunately the results do not correlate with this.

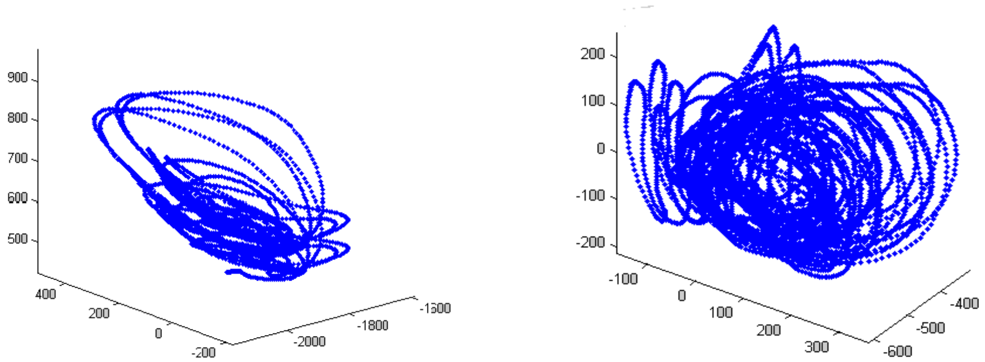

Figure 4.8 - Trajectories of thigh markers in Global and Local Coordinate System

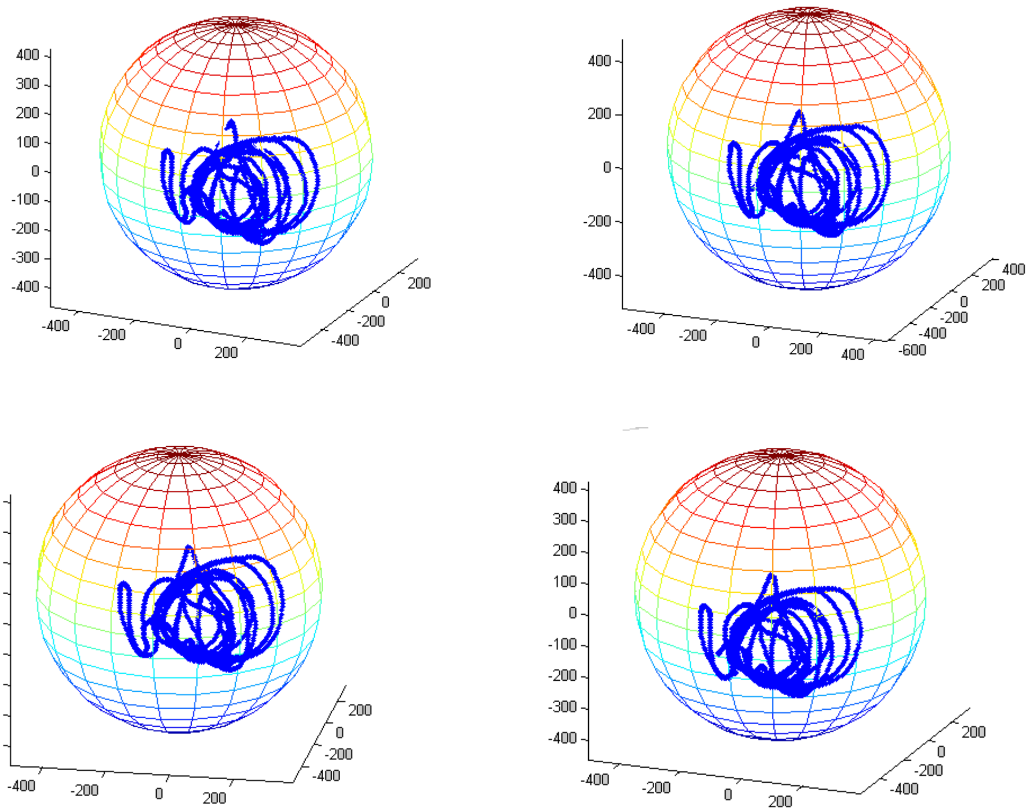

Figure 4.9 - Trajectories of thigh markers on their corresponding spheres in Local Coordinate System

Figures 4.8 and 4.9 above show the thigh markers in global and local coordinate system and on their respective spheres in local coordinate system.

On the other hand, comparing the results with last year results, it is seen that there is a good amount of variation in the coordinates. Centre of rotation from last year results for the same subject was:

$$C = \begin{bmatrix} -36.10 \\ -123.20 \\ -27.43 \end{bmatrix} \text{mm}$$

When compared to MRI results from last year, the difference to the centre found by MRI is smaller for the second and third coordinate but higher for the first coordinate.

4.3. PREDICTIVE RESULTS

The regression equations given by Harrington, et al., (2007) are used for predictive validation of the tests. This is done because as said earlier, the predictive methods remain the most preferred technique in clinical settings for locating HJC. The equations are:

$$X = -0.24PD-9.9$$

$$Y = -0.30PW-10.9$$

$$Z = 0.33PW+7.3$$

Where PD is pelvic depth and PW is pelvic width.

This validation enables to determine whether the predictions are correct or not. The variables for PD and PW are computed by using the data provided by the VICON Nexus software. These were found for both the subjects and the details of the calculations are given below.

4.3.1. SUBJECT 1

1) PD can be described as the distance between the ASIS midpoint and PSIS midpoint. For that, first the midpoints were calculated as follows:

From the Nexus data:

ASIS midpoint = $\left(\frac{x1+x2}{2}, \frac{y1+y2}{2}, \frac{z1+z2}{2}\right)$ …………….. (I)

$= \left(\frac{-1306-1287}{2}, \frac{182-36}{2}, \frac{966+964}{2}\right)$

= (-1296.5, 73, 965)

PSIS midpoint = $\left(\frac{-1130-1129}{2}, \frac{122+32}{2}, \frac{1005+998}{2}\right)$

= (-1129.5, 77, 1001.5)

Distance between the midpoints

PD = $\sqrt{\Delta x2 + \Delta y2 + \Delta z2}$

= $\sqrt{167^2 + 4^2 + 36.5^2}$

= 170.99 mm

2) PW is defined as the distance between the Left and Right ASIS. For that

Δx = -1287 + 1306 = 19

Δy = -36 + 182 = 146

Δz = 964 - 966 = -2

The distance between Left and Right ASIS

PW = $\sqrt{\Delta x2 + \Delta y2 + \Delta z2}$

= $\sqrt{19^2 + 146^2 + (-2)^2}$

= 147.24 mm

Substituting the values of PD and PW in the regression equations:

X = -0.24 (170.99) – 9.9

= -50.94 mm

Y = -0.30 (147.24) – 10.9

= -55.07 mm

Z = 0.33 (147.24) + 7.3

= 55.89 mm

The HJC Coordinates by predictive method are:

$$C = \begin{bmatrix} -50.94 \\ -55.07 \\ 55.89 \end{bmatrix} \text{mm}$$

The above predicted HJC coordinates are relative to the midpoint of PW as origin. Thus, it is necessary to change them into the desired coordinate system in which the right ASIS is the origin. This can be transformed by subtracting the distance in z direction from half of the PW (147.24/2).

Transformed HJC Coordinates relative to right ASIS (considering the sign convention):

$$C = \begin{bmatrix} -50.94 \\ -55.07 \\ -17.73 \end{bmatrix} \text{mm}$$

4.3.2. SUBJECT 2

1) For PD,

ASIS midpoint = $\left(\frac{-1792-1661}{2}, \frac{430+222}{2}, \frac{1021+1016}{2}\right)$ (see eq. (I))

= (-1726.5, 326, 1018.5)

PSIS midpoint = $\left(\frac{-1594-1543}{2}, \frac{468+378}{2}, \frac{1011+1013}{2}\right)$

= (-1568.5, 423, 1012)

The distance between the two midpoints

PD = $\sqrt{\Delta x2 + \Delta y2 + \Delta z2}$

= $\sqrt{159^2 + 97^2 + 6^2}$

= 186.35 mm

2) For PW,

Δx = -1661 + 1792 = 131

$\Delta y \quad = \quad 222 - 430 = -208$

$\Delta z \quad = \quad 1016 - 1021 = -5$

The distance between Left and Right ASIS

$$PW = \sqrt{\Delta x2 + \Delta y2 + \Delta z2}$$

$$= \sqrt{131^2 + (-208)^2 + (-5)^2}$$

$$= 245.87 \text{ mm}$$

Substituting the values of PD and PW in the regression equations:

$$X = -0.24\ (186.35) - 9.9$$

$$= -54.62 \text{ mm}$$

$$Y = -0.30\ (245.87) - 10.9$$

$$= -84.66 \text{ mm}$$

$$Z = 0.33\ (245.87) + 7.3$$

$$= 88.44 \text{ mm}$$

The HJC Coordinates by predictive method are:

$$C = \begin{bmatrix} -54.62 \\ -84.66 \\ 88.44 \end{bmatrix} \text{ mm}$$

Transformed HJC Coordinates relative to right ASIS (considering the sign convention):

$$C = \begin{bmatrix} -54.62 \\ -84.66 \\ -34.50 \end{bmatrix} \text{ mm}$$

It is seen that the difference between the above result and last year result is very negligible. The last year predictive HJC Coordinates were:

$$C = \begin{bmatrix} -55.24 \\ -84.15 \\ -34.35 \end{bmatrix} \text{ mm}$$

The HJC Coordinates for Subject 1 from both the functional and predictive methods show a difference of 5.94 mm and 3.52 mm in x and z direction respectively. But a huge difference of 47.96 mm is seen in the y direction. While that for subject 2 differ by 0.40 mm in x direction but largest variations are seen in y and z directions with 12.69 mm and 14.65 mm respectively. From these comparisons, it is clearly seen that STA is not constant for each individual. The biggest differences occur in different axes for both the subjects with y axis being the common coordinate to vary significantly. These variations emphasize that the methods estimating HJC experience random errors due to various techniques or STA and individual body parameters which should be taken into account for these inaccuracies. The above comparison also highlights the underlying flaws in both predictive and functional methods that still need to be addressed properly before making any accurate prediction.

4.4. ULTRASOUND RESULTS

As described in section 3.4.3, the HJC for subject 2 was estimated last year using ultrasound imaging technique (Simpson, 2011). The results, even though had ASIS as the origin, were based on an orthogonal axis in the frontal plane which had x axis parallel to ground. On the other hand, in functional methods the x axis is defined as the join between ASIS and PSIS midpoints, which is not parallel to ground. Thus, the ultrasound results obtained were transformed to the pelvic axis system by determining the pelvic angle (Simpson 2011).

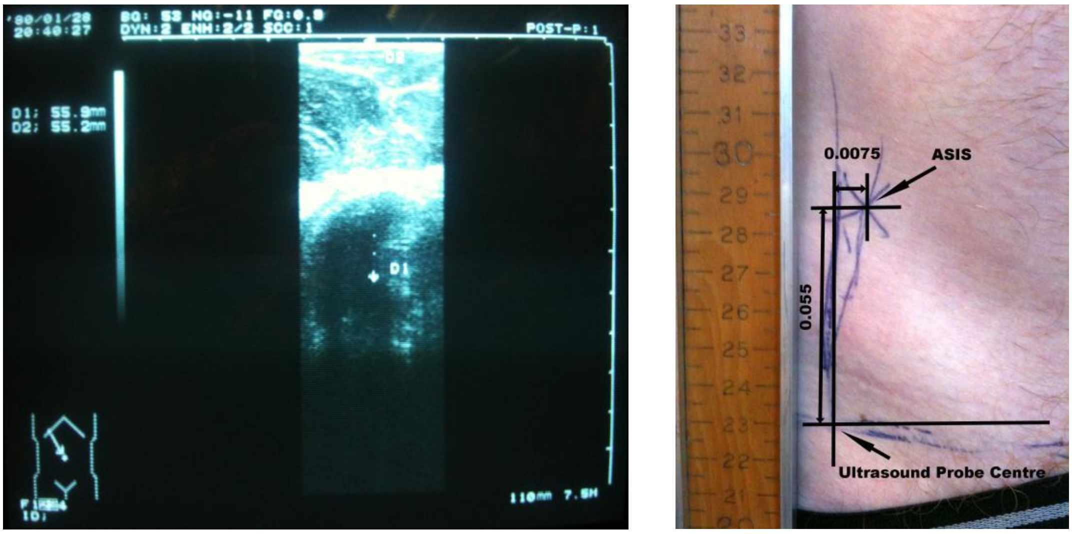

Figure 4.10 - The ultrasound image for subject 2 and the dimensions taken on skin surface (Simpson, 2011)

HJC Coordinates from Ultrasound (Subject 2)

$$C = \begin{bmatrix} -55.51 \\ -72.14 \\ -25.00 \end{bmatrix} \text{mm}$$

When the functional results of present study and study by Simpson, (2011) were compared to the above result, it was observed that the difference between the x and y coordinates of present study result was smaller than that from Simpson's study.

4.5. MRI RESULTS

MRI has been known to provide clear accurate images of the inner structures of the human body that allows better visualisation. The MRI tests performed last year provided very clear images of the Hip Joint Centre. As mentioned earlier in section 3.4.5, the data gathered from the scanner was exported to Mimics 14.12 software which allowed locating bony landmarks and their corresponding distances. The MRI images from the Mimics software along with the HJC coordinates for subject 2 are shown below.

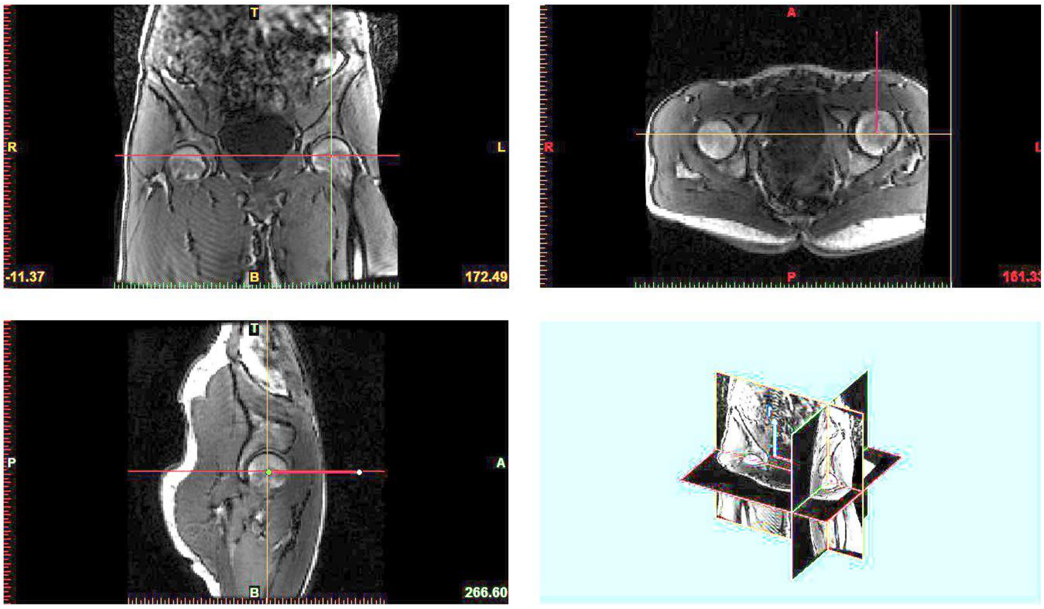

Figure 4.11 – Mimics Screenshots of HJC (Simpson, 2011)

The HJC can be very clearly seen in the above images. The measurements of distances in the frontal plane and angle of pelvis were calculated from these images in order to locate in Local Coordinate System. Measurements were taken from the images that allowed for anatomical positions to be calculated in all slices. Figure 4.12 shows images indicating the distances measured with reference to ASIS in the frontal plane.

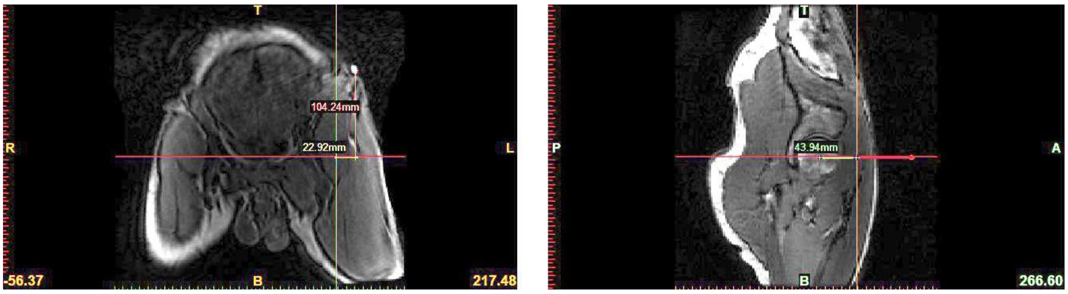

Figure 4.12 – Dimensioned MRI (Simpson, 2011)

HJC Coordinates from MRI

$$C = \begin{bmatrix} -39.47 \\ -105.52 \\ -22.92 \end{bmatrix}$$

Taking the pelvic angle into consideration, the above results were obtained after transforming them into the Local Coordinate System similar to ultrasound results. The software could also create a 3D image using the slices which would have provided better visualization but it was not done last year due to time constraints (Simpson 2011). The results for HJC estimation from MRI were considered to be the true coordinates of the HJC due to its superior image quality.

4.6. COMPILED RESULTS

4.6.1. TABLE FOR SUBJECT 1 RESULTS

FUNCTIONAL METHOD	PREDICTIVE METHOD (Harrington, et al., 2007)
-45.00 -103.03 -21.25	-50.94 -55.07 -17.73

4.6.2. TABLE FOR SUBJECT 2 RESULTS

PRESENT STUDY

FUNCTIONAL METHOD	PREDICTIVE METHOD (Harrington et al. 2007)
-55.02 -97.35 -19.85	-54.62 -84.66 -34.50

SIMPSON'S STUDY (2011)

FUNCTIONAL METHOD	PREDICTIVE METHOD (Harrington et al. 2007)	ULTRASOUND	MRI
-36.10 -123.20 -27.43	-55.24 -84.15 -34.35	-55.51 -72.14 -25.00	-39.47 -105.22 -22.92

From the above results it can be seen that for subject 2, Harrington, et al's (2007) regression equations similar to last year's results produce the largest amount of errors in all the three coordinates. The functional methods suffered from vast amount of errors in x direction but gave improved results in y and z directions than last year. Such varied results are due to the skin tissue artefacts which overall least affect the z coordinates.

4.7. DISCUSSION

This study attempted to reduce the errors in the results from last year and explore ultrasound in more depth. The results from predictive and functional methods can only be compared for subject 2 because no MRI tests were performed for subject 1 due to the cost factor associated with the test. Comparison of the functional and predictive methods with MRI for subject 2 proved the results to be far from accurate for both methods but showed improvements in y and z coordinates for results from functional method. The functional method worked well with the mechanical model but did not have any significant improvement for subject tests. The one main factor leading to these vast amounts of errors is the skin tissue artefacts which are not easy to eliminate. They differ for each individual and affect every marker position (hip and thigh) on the subject. Placing the markers is also very critical for getting accurate results. This is not an easy task because the bony landmarks are not points but curvatures of the bones which may become hard to palpate and find if the individual is not skinny. It is not possible to maintain the level of consistency in positioning the markers because it depends on the supposed location of the pelvic bony landmarks that can vary from their true position. The errors while positioning of markers can be up to some mm which reduce the precision of the Local Coordinate System significantly.

The ultrasound images obtained from subject 1 are an example for future improvement to reconstruct 3D image from 2D ultrasound images. The femur could be easily seen in the ultrasound images and with the slices technique a 3D reconstruction would be very effective. The ultrasound results obtained for subject 2 by Simpson (2011) were very unclear and probably suffered from a number of errors. This study tried to overcome those errors by using a high-end ultrasound scanner machine and the imaging being done by an expert. It is found that the images for subject 1 are more informative and clear than the images for subject 2.

CHAPTER 5.

CONCLUSION

It can be concluded from the results of the study that the functional methods have improved the predictions greatly but the exact location of HJC is still far from accurate. The validation techniques are also found to be inaccurate due to the effect of soft tissue artefacts. MRI is costly hence ultrasound is used which is found to have good potential but it still needs a better equipment to determine the location of HJC accurately. The most surprising result that is seen from this study is that, the Harrington, et al's (2007) regression equations that are widely used in the clinical settings, proved to be the least accurate.

Ultrasound has a potential to become the new gold standard for imaging surfaces of bones. MATALB software can be used to create a program that uses multiple 2D ultrasound images to reconstruct a 3D image. For future, the technique used to obtain these images (slices at different positions or angular images) can be explored in detail. All these developments indicate that ultrasound if carried out with better equipment by an expert of the field can yield very useful results.

CHAPTER 6.

FUTURE WORK

Ultrasound initially was used to image soft tissues inside the body. But now it is being used to image bones too. Bony tissues do not allow ultrasound to pass through it which forms a very bright white image on the screen. This study shows that there is a lot of scope of improvement in using ultrasound imaging technique for locating the Hip Joint Centre. Ultrasound just like other validation techniques also suffers from skin tissue artefacts. Thus, emphasis should be given on reducing it when imaging the HJC. This can be achieved by using a water bath for ultrasound imaging. In this, the subject is made to stand in a water bath and the ultrasound transducer is placed at a distance from the subject. The subject stands still in the bath and the transducer is made to move around the area of interest-in this case the hip joint, and generate 2D ultrasonic images obtained from different angles. The transducer movement is controlled by a stepper motor. There is no contact of the probe with the subject’s skin which eliminates the skin tissue artefacts that arise due to the probe contact. This technique has been applied for the emergency ultrasound of patients in hospitals and studies proved it to be very useful in obtaining a superior quality image without any discomfort to the patients (Blaivas, et al., 2004).

Secondly, the machine used for ultrasound imaging in this study is a 2D machine. A 3D machine can provide better results in locating the HJC. It has built-in software which allows the user to view a real time ultrasound 3D image on the monitor. The Frame Graber software along with any 3D reconstruction software can be applied as an initial effort to obtain a 3D image from numerous 2D ultrasound images. Figure 6.1 shows a 3D image of a femur head after being reconstructed.

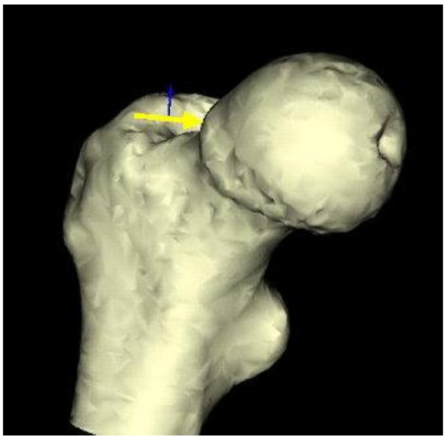

Figure 6.1 – 3D-reconstruction of the top of the femur (McDermott, 2010)

Further, although the functional methods provide results with less amount of error than predictive methods but they still are affected by skin tissue artefacts. Further investigations must be carried out to establish a relationship between the skin tissue artefacts and the HJC coordinates.

The following approaches could be adopted to obtain 3D ultrasound images.

There are four categories in which 3D ultrasound image acquisition approaches can be classified (The Hong Kong Polytechnic University, 2011):

1. Systems with 2-D transducer arrays that produce 3D images in real-time of volume of interest. They are costly and not available easily.

2. Mechanical scanners where moving the transducers in rotation/translation manner provide the position data from stepper motors in the scanning heads. The scans can be placed in parallel slices arrangement using linear motion, a wedge by means of tilt motion, or a cone or cylinder with rotational motion.

3. Freehand methods with positional information. The position sensing devices are used to record the position and orientation of the probe and then to reconstruct 3D data set.

4. Freehand methods without positional information. The position sensing devices are not used in these systems. Relative positions and orientations among B-scans are estimated from the information derived from images.

The last approach requires smooth movement of the probe in one direction avoiding any rotational and translational movements between B-scans. Owing to the errors introduced by the movement during data acquisition, this approach does not provide accurate measurements. The third approach is the most popular amongst all as it offers free hand operation for clinical applications. It comprises of 3 primary parts: a 2D ultrasound scanner, a 3D space locator and a computer. The scanner acquires 2D data, the space locator measures the probe position and orientation and the computer is equipped with the required software to assemble spatial data and 2D images along with reconstructing and displaying 3D images and analysing volume data.

The figures 6.2 – 6.8 below are obtained from an ultrasound scanner by ZONARE with a transducer having a variable resolution between 10 – 5 MHz installed at the Ninewells Hospital, Dundee. These pictures show the ultrasound images of the femur of subject 1 which were captured at a frequency of 6.0 MHz. The pictures also show the depth at which these screenshots were taken. If seen clearly the order of the pictures shows the femur from the shaft to the neck to the head. The transducer is placed on the lateral plane of the thigh showing the shaft of the femur and is moved upwards laterally to obtain the image of the femur head. These images are an example of how a 3D image can be obtained. By taking images in form of slices at set distances over the thigh and the hip (for example – 10 mm), a 3D image of the hip can be obtained by using MATLAB program. The areas of interest can be marked in each image and the program superimposes all the images on each other identifying every marking on every image to create a 3D view. There is another way of obtaining 2D images for 3D reconstruction. The transducer needs to be moved in angular manner at one point to obtain images at different angles at the same point. This technique suffers from a drawback of being very difficult to implement. The images are difficult to obtain in this manner as it requires a very stable hand during probe movement. The concept of the ultrasound images in form of slices at set distances is similar to the CT imaging technique. CT takes slices of the area of interest at different angles and location which then appear as 3D view of the area. The MATLAB program performs a similar task of obtaining a 3D image from multiple 2D images. This could not be accomplished for the present study due to lack of time.

Figure 6.2 shows the shaft of the femur. The position of the transducer is at the mid thigh on the lateral border.

Figure 6.3 and Figure 6.4 are the images approximately at a distance of 10 mm from Figure 1 with the transducer at the lateral border of thigh closer to the hip. It can be seen the shaft becomes clearer along with its borders.

In Figure 6.5 the neck of the femur is clearly visible. At this point the transducer is very close to the lateral side of the hip. As mentioned before, subject 1 is very skinny and the hip joint could be easily located from the lateral side. This is evident in

Figure 6.5 as the image of the neck of femur is very clear which indicates less amount of fat present.

Finally the Figure 6.6 shows the round dark area which is the femur head. It is a dark shadow because the ultrasound waves cannot pass through the bone and it appears as a black shadow instead.

Figure 6.7 and Figure 6.8 are taken from the medial side of the thigh showing the inner border of the femur. It is seen that the image becomes unclear as the probe is moved up towards the pubic symphysis.

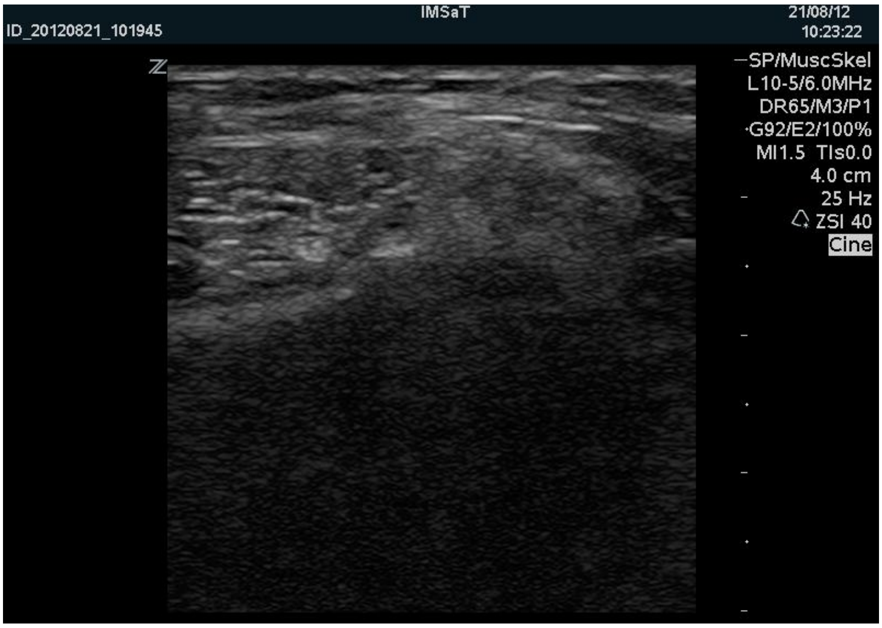

Figure 6.2 - The borders of the femur can be seen on the extreme left of the picture.

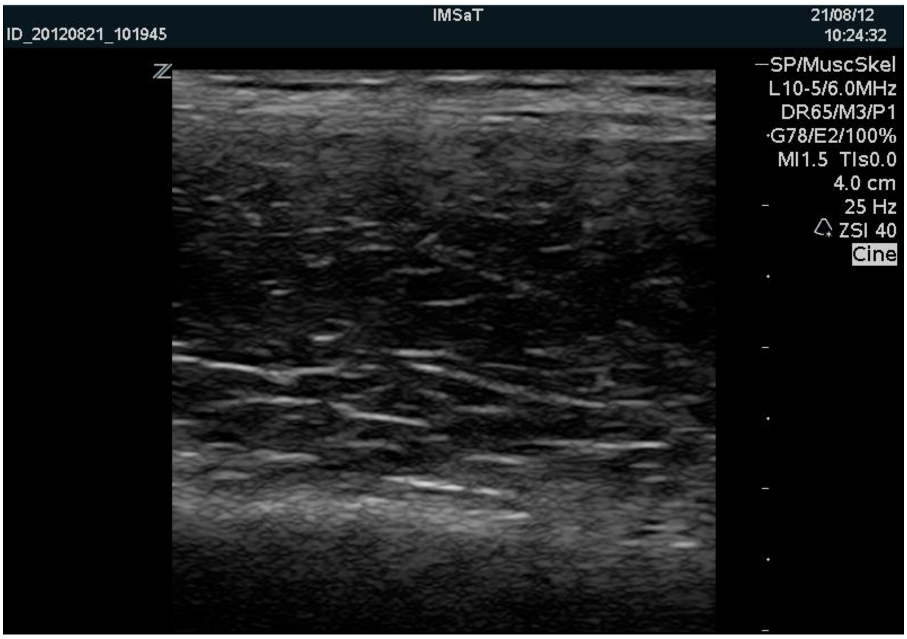

Figure 6.3 - The shaft of femur is clearly visible with the border seen in the lower half of the picture.

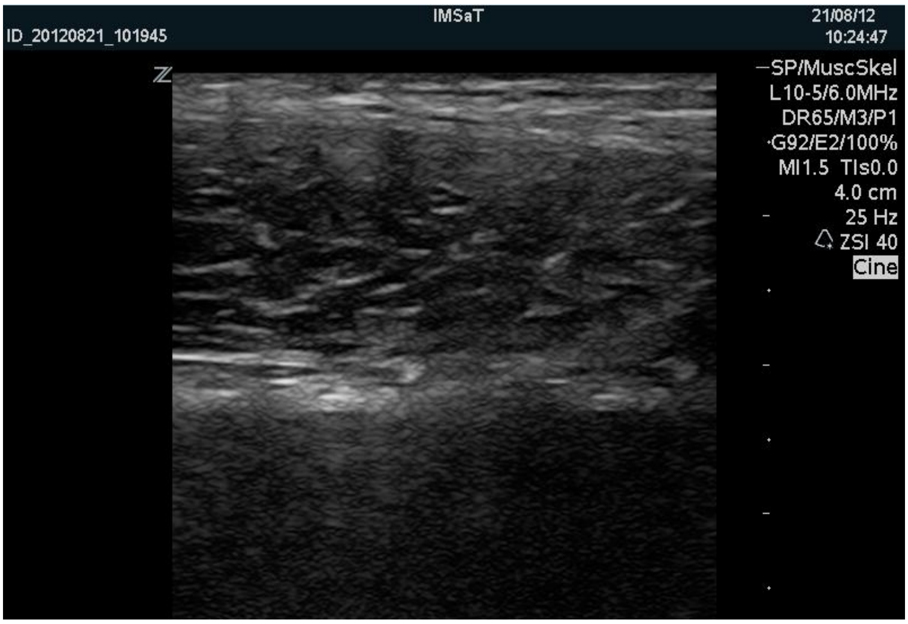

Figure 6.4 - Screenshot showing the femur shaft at a different section (closer to the femur head).

Figure 6.5 - Neck of the femur is clearly visible.

Figure 6.6 - The femur head.

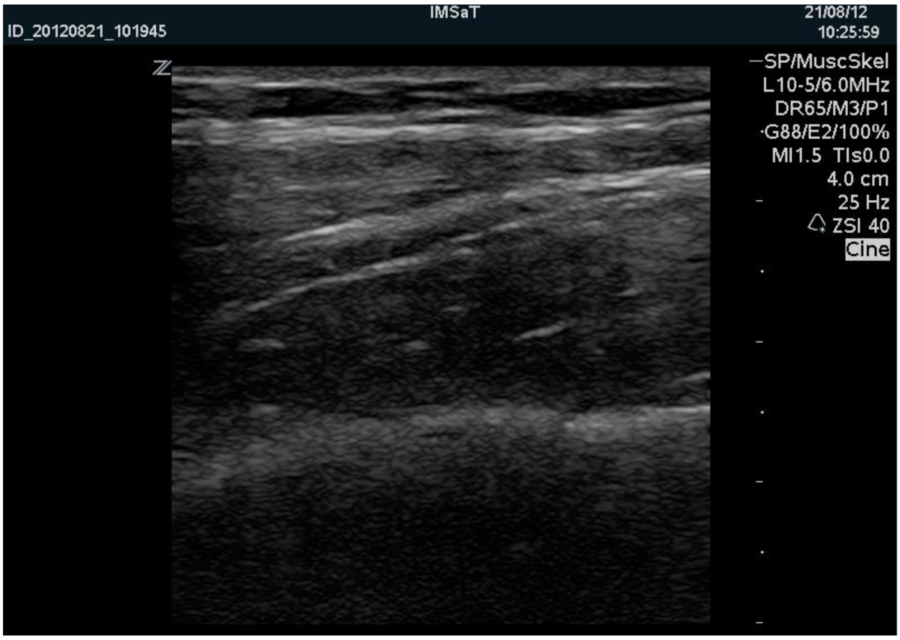

Figure 6.7 - Inner border of the femur shaft

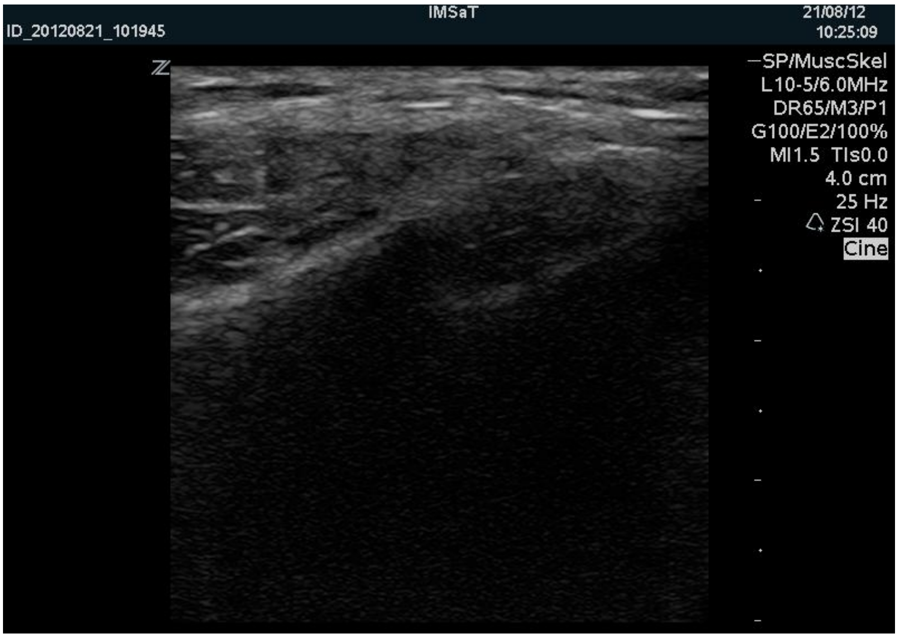

Figure 6.8 - Inner border of the femur shat disappearing

REFERENCES

- Bell, A., Brand, R. & Pedersen, D., 1989. Prediction of hip joint center location from external landmarks.. *Human Movement science,* Volume 8, pp. 3-16.

- Bell, A., Pedersen, D. & Brand, R., 1990. A comparison of the accuracy of several hip center location prediction methods.. *Journal of Biomechanics ,* Volume 23, pp. 617-621..

- Blaivas, M. et al., 2004. Water bath evaluation technique for emergency ultrasound of painful superficial structures. *The American Journal of Emergency Medicine*, 22(7), p. 589–593.

- Cereatti, A. et al., 2009. Hip joint centre location: An ex vivo study. *Journal of Biomechanics,* Volume 42, pp. 818-823.

- Davis, R., Õunpuu, S., Tyburski, D. & Gage, J., 1991. A gait analysis data collection and reduction technique. *Human Movement Science,* 10 (5), p. 575–587.

- Gamage, S. & Lasenby, J., 2002. New least squares solutions for estimating the average centre of rotation and axis of rotation. *Journal of Biomechanics 35 p87-93,* Volume 35, pp. 87-93.

- Harrington, M. et al., 2007. Prediction of the hip joint centre in adults, children and patients with cerebral palsy based on magnetic resonance imaging. *Journal of Biomechanics 40 p595-602,* 40(3), pp. 595-602.

- Leardini, A. et al., 1999. Validation of a functional method for estimation of hip joint centre location. *Journal of Biomechanics,* Volume 32, pp. 99-103.

- Lucchetti, L., Cappozo, A., Cappello, A. & Croce, U., 1998. Skin movement artefact assessment and compensation in the estimation of knee-joint kinematics. *Journal of Biomechanics,* Volume 31, pp. 977-984.

- Martini, F. & Nath, J., 2009. The Hip Joint. In: *Fundamentals of Anatomy & Physiology.* s.l.: Benjamin Cummings; , p. 283.

- McDermott, I., 2010. *London Sports Orthopaedics-Hip Impingement.* [Online]
  Available at: http://www.sportsortho.co.uk/left-navigation/conditions/hip/hip-impingement
  [Accessed 13 April 2012].

- Mechlenburg, I., Nyengaard, J., Gelineck, J. & Soballe, K., 2007. Cartilage thickness in the hip joint measured by MRI and stereology – a methodological study. *Osteoarthritis and Cartilage,* 15(4), p. 366–371.

- Nötzli, H. et al., 2002. The contour of the femoral head-neck junction as a predictor for the risk of anterior impingement. *The Journal of Bone and Joint Surgery,* 84-B(4), pp. 556-560.

- Peters, A., 2010. *Gait analysis methods to minimise soft tissue artefact and evaluate techniques to locate the hip joint centre,* PhD Thesis, Medicine, Dentistry & Health Sciences - Physiotherapy, : University of Melbourne.

- Peters, A., Baker, R. & Sangeux, M., 2010. Validation of 3-D freehand ultrasound for the determination of the hip joint centre. *Gait and Posture,* 31(4), p. 530–532.

- Ryu, T., Choi, H. S. & Chung, M. K., 2009. Soft tissue artifact compensation using displacement dependency between anatomical landmarks and skin markers – a preliminary study. *International Journal of Industrial Ergonomics,* 39(1), pp. 152-158.

- Seidel, G. K., Marchinda, D. M., Dijkers, M. & Soutas-Little, R. W., 1995. Hip Joint Center Location From Palpable Bony Landmarks-A Cadaver Study. *Journal of Biomechanics,* 28(8), pp. 995-998.

- Simpson, C., 2011. *Prediction of the Hip Joint Centre from Externally Placed Markers in Gait Analysis Studies,* Glasgow: University of Strathclyde,.

- Siston, R. A. & Delp, S. L., 2006. Evaluation of a new algorithm to determine the hip joint center. *Journal of Biomechanics,* 39(1), pp. 125-130.

- Stagni, R., Fantozzi, S., Cappello, A. & Leardini, A., 2005. Quantification of soft tissue artefact in motion analysis by combining 3D fluoroscopy and stereophotogrammetry: a study on two subjects. *Clinical Biomechanics,* 20(3), pp. 320-329.

- The Hong Kong Polytechnic University, 2011. *3D Ultrasound Imaging.* [Online]

  Available at: www.acad.polyu.edu.hk/~rcbus/3DUltrasoundImaging/Introduction.htm [Accessed 27 July 2012].

- Wu, G. et al., 2002. ISB recommendation on definitions of joint coordinate system of various joints for reporting of human joint motion – part I: ankle,hip, spine. *Journal of Biomechanics,* Volume 35, pp. 543-548.

- Yu, H., Pattichis, M. S., Agurto, C. & Goens, M. B., 2011. A 3D Freehand Ultrasound System for Multi-view Reconstructions from Sparse 2D Scanning Planes. *Biomedical Engineering online,* 10(7), pp. 1-22.

APPENDIX- MATLAB Program and functions

The program below uses the data collected from the mechanical model as well as from both the subjects. Then a local coordinate system is created with the 4 hip markers to transfer the leg marker trajectories into this system. The program output is the predicted coordinates of the HJC in local coordinate system.

The functions used in the final script and the code for Gamage and Lasenby are listed further on which the whole program is based.

Final Script

```
%% clean the workspace
hold off
clear all
close all

flag = 2; %1 for mechanical part, 2 for subject data
number_tracks = 4;
split_flag = 0; %change to 1 to do splitting
track_centre = 0;

if flag == 1

 %% load the data:
 % the matrix P of all points and indices of the tracks

 %Taranjit's mechanical model data ("new")
 mech_model_new_trial_2
 number_tracks = 4;
 track_centre = 1;

 %% extract tracks
 % thigh tracks
 %  T(:,:,1)=P(:,T1ind);
 for i=1:number_tracks
  T(:,:,i)=P(:,eval(['T',int2str(i),'ind']));
 end
 % hip tracks
 H(:,:,1)=P(:,H1ind);
 H(:,:,2)=P(:,H2ind);
 H(:,:,3)=P(:,H3ind);

 % centre in absolute coordinates
 CE = H(:,:,1);

 %% coordinate transformation
 % compute the coordinate vectors using the hip tracks
 [s1 s2 s3] = coordinate_vectors (H(:,:,1),H(:,:,2),H(:,:,3));
```

```
elseif  flag == 2

%  %Taranjit's subject data
  subject2_trial_4
  number_tracks = 4;


%  %Taranjit's mechanical model data ("rigid")
%  mech_model_rigid_trial_4
%  number_tracks = 4;

%  %Taranjit's mechanical model data ("non-rigid")
%  mech_model_trial_4
%  number_tracks = 6;

 %Taranjit's mechanical model data ("new")
% mech_model_new2_trial_1
% number_tracks = 4;
% track_centre = 1;

 %% extract tracks
 % thigh tracks
 %  T(:,:,1)=P(:,T1ind);
 for i=1:number_tracks
  T(:,:,i)=P(:,eval(['T',int2str(i),'ind']));
 end



 % hip tracks
 F1=P(:,F1ind);
 F2=P(:,F2ind);
 R1=P(:,R1ind);
 R2=P(:,R2ind);

 % centre of the relative ("hip") coordinate system in absolute
coordinates
 CE=F1;

 %% coordinate transformation
 % compute the coordinate vectors using the hip tracks
 [s1 s2 s3] = coordinate_vectors_hip (F1,F2,R1,R2);
 %[s1 s2 s3] = coordinate_vectors (F1,F2,R1);

end

% transform the thigh tracks into the relative coordinate system
for i=1:number_tracks
  Pr(:,3*i-2:3*i) = relative_coordinates (T(:,:,i),CE,s1,s2,s3);
%T(:,:,i); %to use absolute coordinates
end

% splitting
if split_flag == 1
%     %split in two
%     Pr = [Pr(1:456,:) Pr(457:912,:)];
     %split in three
```

```
    Pr = [Pr(1:304,:) Pr(305:608,:) Pr(609:912,:)];

%     %split in three and remove some points
%     Pr = [Pr(1:300,:) Pr(301:600,:) Pr(601:900,:)];
end

 disp(' ')

%compute the centre by using the two "ball tracks" (Taranjit's "new"
mechanical model data)
if track_centre == 1
 %compute absolute coordinates of the centre
 C1 = P(:,C1ind);
 C2 = P(:,C2ind);
 Ca=(C1+C2)/2;

%  %debugging
%  disp('centre in absolute coordinates estimated from ball
markers:')
%  disp('   average   minimum   maximum   max-min')
%  disp([sum(Ca)/size(Ca,1); min(Ca); max(Ca); max(Ca)-min(Ca)]')
 %% plot the original ball tracks in absolute coordinates
 figure(100)
 plot3(C1(:,1),C1(:,2),C1(:,3),'.')
 hold on
 plot3(C2(:,1),C2(:,2),C2(:,3),'.')
 plot3(Ca(:,1),Ca(:,2),Ca(:,3),'r.')
 axis equal
 axis tight

 %transform the ball tracks and centre into relative coordinates
 C1r=relative_coordinates (C1,CE,s1,s2,s3);
 C2r=relative_coordinates (C2,CE,s1,s2,s3);
 Cr=relative_coordinates (Ca,CE,s1,s2,s3);

 %% plot the ball tracks in relative coordinates
 figure(101)
 plot3(C1r(:,1),C1r(:,2),C1r(:,3),'.')
 hold on
 plot3(C2r(:,1),C2r(:,2),C2r(:,3),'.')
 plot3(Cr(:,1),Cr(:,2),Cr(:,3),'r.')
 axis equal
 axis tight

 disp('centre estimated from ball markers:')
 disp('   average   minimum   maximum   max-min')
 Cr_ave = sum(Cr)/size(Cr,1);
 disp([Cr_ave; min(Cr); max(Cr); max(Cr)-min(Cr)]')

 %estimate the radii of the spheres using the centre from "ball
tracks"
 for i=1:number_tracks
   tmp = Pr(:,3*i-2:3*i) -Cr;
     tmp = tmp.*tmp;
     tmp = sqrt(sum(tmp'));
   rb(i) = sum(tmp')/length(tmp);
 end
```

```
 disp('radii estimated from ball markers:')
 disp(rb)
 disp('Accuracy of the ball marker sphere fit for each track and
distances to the centre')
 disp('             rms error    bias     ave_dist   min_dist
max_dist')
 n=size(Pr,1); % number of points
 for i=1:number_tracks
   diffs = Pr(:,3*i-2:3*i) - ones(n,1)*Cr_ave;
     dists = sqrt(sum(diffs.*diffs,2)); %distances to the computed
centre
     ave_dist = sum(dists)/length(dists);
     max_dist = max(dists);
     min_dist = min(dists);
     rad_rms = sqrt(sum((dists - rb(i)).^2)/n);
     rad_bias = sum(dists)/n - rb(i);
     disp([int2str(i),'-th track:   ',num2str(rad_rms,'%.4f'),'
',num2str(rad_bias,'%.2e'),...
           '   ',num2str(ave_dist,'%.4f'),'
',num2str(min_dist,'%.4f'),'   ',num2str(max_dist,'%.4f')])
 end

end


% find the centre of rotation and radii
[c r A b] = GamageLasenby(Pr);
disp(' ')
disp('centre estimated by Gamage/Lasenby:')
disp(c)
disp('radii estimated by Gamage/Lasenby:')
disp(r)

if track_centre == 1
  disp('difference between centre estimated by ball markers and
Gamage/Lasenby:')
  disp([sum(Cr)/size(Cr,1)]'-c)
  disp('difference between radii estimated by ball markers and
Gamage/Lasenby:')
  disp(rb-r)
end

%% generate the spheres
% points of the unit sphere
[X,Y,Z] = sphere(20);
% expand to the radius r and shift to the centre c
for i=1:number_tracks
  XX(:,:,i) = X*r(i) + c(1);
    YY(:,:,i) = Y*r(i) + c(2);
    ZZ(:,:,i) = Z*r(i) + c(3);
end


%% plot some of the original thigh tracks
figure(1)
for i=1:2
 plot3(T(:,1,i),T(:,2,i),T(:,3,i),'.')
 hold on
```

```
 axis equal
end
axis tight

%% plot all thigh data in relative coordinates
figure(2)
hold on
for i=1:number_tracks
  plot3(Pr(:,3*i-2),Pr(:,3*i-1),Pr(:,3*i),'.')
end
axis equal
axis tight

%% plot each thigh track with the sphere
for i=1:number_tracks
    figure
    plot3(Pr(:,3*i-2),Pr(:,3*i-1),Pr(:,3*i),'.')
    hold on
    mesh(XX(:,:,i),YY(:,:,i),ZZ(:,:,i))
  axis equal
  axis tight
end



%% Assesment
disp(['condition number of A: ',num2str(cond(A))])
disp(' ')
disp('Accuracy of the sphere fit for each track and distances to the
centre')
disp('              rms error    bias      ave_dist   min_dist
max_dist')
n=size(Pr,1); % number of points
for i=1:number_tracks
  diffs = Pr(:,3*i-2:3*i) - ones(n,1)*c';
    dists = sqrt(sum(diffs.*diffs,2)); %distances to the computed
centre
    ave_dist = sum(dists)/length(dists);
    max_dist = max(dists);
    min_dist = min(dists);
    rad_rms = sqrt(sum((dists - r(i)).^2)/n);
    rad_bias = sum(dists)/n - r(i);
    disp([int2str(i),'-th track:   ',num2str(rad_rms,'%.4f'),'
',num2str(rad_bias,'%.2e'),...
          '    ',num2str(ave_dist,'%.4f'),'
',num2str(min_dist,'%.4f'),'   ',num2str(max_dist,'%.4f')])
end

if flag == 1

 %% plot all hip tracks and the track of the computed centre
 figure
 hold on
 for i=1:3
   plot3(H(:,1,i),H(:,2,i),H(:,3,i),'.')
 end
 cabs = absolute_coordinates (ones(n,1)*c',CE,s1,s2,s3);
 plot3(cabs(:,1),cabs(:,2),cabs(:,3),'r')
 axis equal
```

```
 axis tight

end
disp(' ')

% %% plot the hip data in relative coordinates (needed for debugging
only)
% each track must collapse into one point
% figure(356)
% for i=5:7
%   Pr(:,3*i-2:3*i) = relative_coordinates (P(:,3*i-
2:3*i),H(:,:,1),s1,s2,s3);
%   plot3(Pr(:,3*i-2),Pr(:,3*i-1),Pr(:,3*i),'.r')
%   hold on
% end
% axis equal
% axis tight
```

Absolute Coordinates

```
function pnew = absolute_coordinates (p,c,s1,s2,s3)
% given n points in relative coordinates and the relative coordinate
system for each,
% compute the absolute coordinates of all points
%   p -- an (n x 3)-matrix whose rows are relative coordinates to be
transformed
%   c -- an (n x 3)-matrix whose rows are absolute coordinates of
the origins of the
%        relative coordinate systems
% s1,s2,s3 -- (n x 3)-matrices of unit vectors of the relative
coordinate systems
%  pnew -- the (n x 3)-matrix of absolute coordinates
%
% Oleg Davydov 04/06/2010

% for each moment, the transformation matrix is the transpose of the
matrix given by s1,s2,s3,
% and the coordiantes of the absolute unit vectors are the columns
of this matrix:
t1 = [s1(:,1) s2(:,1) s3(:,1)];
t2 = [s1(:,2) s2(:,2) s3(:,2)];
t3 = [s1(:,3) s2(:,3) s3(:,3)];

% find the relative coordinates of the origin of the absolute system
cnew = -[sum(c.*s1,2) sum(c.*s2,2) sum(c.*s3,2)];

% the coordinates are the inner products of p-cnew with t1,t2,t3
p=p-cnew;
pnew = [sum(p.*t1,2) sum(p.*t2,2) sum(p.*t3,2)];
```

Relative Coordinates

```
function pnew = relative_coordinates (p,c,s1,s2,s3)
% given n points in absolute coordinates and the relative coordinate
system for each,
% compute the relative coordinates of all points
%   p -- an (n x 3)-matrix whose rows are absolute coordinates to be
transformed
%   c -- an (n x 3)-matrix whose rows are absolute coordinates of
the origins of the
%        relative coordinate systems
% s1,s2,s3 -- (n x 3)-matrices of unit vectors of the relative
coordinate systems
%  pnew -- the (n x 3)-matrix of relative coordinates
%
% Oleg Davydov 02/06/2010


% the coordinates are the inner products of p-c with s1,s2,s3
p=p-c;
pnew = [sum(p.*s1,2) sum(p.*s2,2) sum(p.*s3,2)] ;
```

Coordinate Vectors

```
function [s1 s2 s3] = coordinate_vectors (p1,p2,p3)
% computes three arrays of unit coordinate vectors from three arrays
of 3D points
% p1,p2,p3 - (n x 3)-matrices containing for each n the coordinates
of three points in the space
% s1,s2,s3 - (n x 3)-matrices containing for each n the coordinates
of three unit vectors that
%            build an orthogonal coordinate system generated by
orthogonalising p2-p1 and p3-p1,
%            and adding their cross product
% The origins of the new coordinate systems will be at p1
% Assumes that the points in the rows of p1,p2,p3 are not collinear
%
% Oleg Davydov 04/06/2010


%% compute the first coordinate directions as difference of p2 and
p1
s1=p2-p1;
s1=normalise(s1); %normalisation

%% compute the second coordinate directions by orthogonalising the
difference p3-p1
s2=p3-p1;
pr = sum(s2.*s1,2); % compute projections on s1
s2=s2-s1.*pr(:,[1 1 1]);% orthogonalisation of s2
s2=normalise(s2);

% compute the third coordinate directions using the cross product
s3 = cross(s1,s2,2);
s3=normalise(s3);
function v = normalise(v)
```

```
% normalise each row of an (n x 3)-matrix

norms = sqrt(sum(v.*v,2));
v=v./norms(:,[1 1 1]);
%v=v./norms(:,ones(3, 1));
```

Rotation Matrix

```
function R=rotation_matrix3D(a,b,c)
%3D rotation matrix with Euler angles a,b,c
%http://en.wikipedia.org/wiki/Rotation_matrix

Rx=[1 0 0; 0 cos(b) -sin(b); 0 sin(b) cos(b)];
Ry=[cos(a) 0 sin(a); 0 1 0; -sin(a) 0 cos(a)];
Rz=[cos(c) -sin(c) 0; sin(c) cos(c) 0; 0 0 1];
R=Rz*Rx*Ry;
```

Coordinate Vectors - Hip

```
function [s1 s2 s3] = coordinate_vectors_hip (f1,f2,r1,r2)
% computes three arrays of unit coordinate vectors from three arrays
of 3D points
% f1,f2,r1,r2 - (n x 3)-matrices containing for each n the
coordinates of the two front (f1,f2)
%             and two rear (r1,r2) markers on the hip
% s1,s2,s3 - (n x 3)-matrices containing for each n the coordinates
of three unit vectors that
%             build an orthogonal coordinate system generated by
orthogonalising p2-p1 and p3-p1,
%             and adding their cross product
% The origins of the new coordinate systems will be at f1
% Assumes that the points in the rows of p1,p2,p3 are not collinear
%
% Oleg Davydov 25/07/2010


%% compute the third coordinate directions (z-axis) as difference of
f2 and f1
z=f1-f2;
z=normalise(z); %normalisation

%% compute the first coordinate directions (x-axis)
x=(f1+f2-r1-r2)/2;

% orthogonalise x to z; comment out the next two lines to discard
orthogonalisation
pr = sum(x.*z,2); % compute projections on z
x=x-z.*pr(:,[1 1 1]);% orthogonalisation of x

%normilise x
x=normalise(x);
```

```
%% compute the second coordinate directions (y-axis) using the cross
product
y = cross(z,x,2);
y=normalise(y);

s1=x;
s2=y;
s3=z;


function v = normalise(v)
% normalise each row of an (n x 3)-matrix

norms = sqrt(sum(v.*v,2));
v=v./norms(:,[1 1 1]);
%v=v./norms(:,ones(3, 1));
```

Gamage Lasenby

```
function [c r A b] = GamageLasenby(P)
% Computing the centre of rotation from a number of tracks on
concentric spheres
%
% Reads a matrix P of size n x 3p, where p is the number of tracks
% and n the number of points in each track.
% In each track, the three consecutive columns correspond to x-, y-
and z-coordinates.
%
% Returns:
%   c -- the coordinates of the centre of rotation
%   r -- the p-vector of radii of the spheres of the tracks
%  A,b -- the matrix and RHS of the linear system to investigate
numerical stability
%
% Oleg Davydov 04/06/2010

% number of points in  the tracks
n = size(P,1);

% number of tracks
p = size(P,2)/3;

%% various averages and outer products for all tracks
av = reshape(mean(P),3,[]);
PP = P.*P; % squares of all entries of P
%av2 = sum(reshape(sum(PP),3,[]))/n;
av2 = zeros(1,p);
av3 = zeros(3,p);
Avop = zeros(3,3*p); %outer products of averages
Pt=P';
Pop=zeros(3*n,3*p); % outer products of the points in 3x3-blocks
for i=1:p
  indx = 3*i-2:3*i;
  sqn=sum(PP(:,indx),2);% squared norms of all points of the p-th
track
    av2(i) = sum(sqn)/n;
```

```
    av3(:,i) = sum(P(:,indx).*sqn(:,[1 1 1]))'/n;
    tav = av(:,i);
    Avop(:,indx)=tav*tav';
  Pop(:,indx(1))=reshape(Pt(indx,:),3*n,1);
  Pop(:,indx(2))=reshape(Pt(indx,:),3*n,1);
  Pop(:,indx(3))=reshape(Pt(indx,:),3*n,1);
end
Pop=Pop.*P(reshape([1:n; 1:n; 1:n],3*n,1),:); % contains the outer
products in 3x3-blocks

%% setting up the linear system
% RHS
b = sum(av3 - av.*av2([1; 1; 1],:),2);
% sum up the outer product matrices in columns, average and subtract
the matrix avop
Sop=[sum(Pop(1:3:3*n-2,:)); sum(Pop(2:3:3*n-1,:));
sum(Pop(3:3:3*n,:))]/n - Avop;
% sum up in rows to obtain the matrix of the linear system
A=2*[sum(Sop(:,1:3:3*p-2),2) sum(Sop(:,2:3:3*p-1),2)
sum(Sop(:,3:3:3*p),2)];

% solve the linear system to obtain the centre or rotation
c=A\b;

% find the radii
P=P-c(ones(n,1)*reshape([ones(1,p); 2*ones(1,p);
3*ones(1,p)],1,3*p));
P = P.*P;
r = sqrt(sum(reshape(sum(P),3,p))/n);
```